Performance Analysis of Multi-RIS-Aided LoRa Systems With Outdated and Imperfect CSI

Zhaokun Liang, Guofa Cai, *Senior Member, IEEE*, Jiguang He, *Senior Member, IEEE*, Georges Kaddoum, *Senior Member, IEEE*, and Chongwen Huang, *Member, IEEE*

***Abstract*— Although LoRa has emerged as the leading technology among the rapidly developing low-power wide-area networks, the performance of the LoRa system severely deteriorates over fading channels. To address this problem, in this paper, we introduce multiple reconfigurable intelligent surfaces (multi-RISs) into the LoRa system to improve its performance. Our specific focus is on the impact of outdated channel state information (CSI), the imperfection of estimated CSI, and the design of RIS discrete phase shifts on the performance. To this end, we first use the moment-matching method to obtain the end-to-end (E2E) channel coefficient of the joint outdated channels and erroneous channels over Nakagami-m fading. Moreover, the closed-form bit error rates (BERs) of the proposed system with non-coherent and coherent detections are derived. The results reveal that, in the high signal-to-noise ratio (SNR) regime, coherent detection encounters the error floor and performs worse than non-coherent detection. Furthermore, we also analyze delay outage rate, throughput, and achievable diversity order of the proposed system. The results show that, despite the presence of outdated CSI and channel estimation errors, the proposed system is still superior to RIS-aided LoRa systems adopting blind transmission and RIS-free ones. Finally, we also thoroughly investigate the effects of various important factors such as the correlation factor, channel estimation errors, the number of RIS reflecting elements, and the number of quantization bits for RIS discrete phase shifts on the performance.**

***Index Terms*— LoRa network, reconfigurable intelligent surfaces (RISs), discrete phase shift design, outdated channel state information (CSI), bit error rate (BER), delay outage rate, throughput.**

Received 27 May 2024; revised 28 September 2024; accepted 1 December 2024. Date of publication 5 December 2024; date of current version 17 July 2035. This paper was supported by the NSF of China under Grant 62071129, 62331023, 62101492, 62394292 and U20A20158; in part by the Guangdong Special Support Program for Young Top notch Talents Project under Grant 2023TQ07X481; in part by the NSF of Guangdong Province under Grant 2025A1515010128; in part by the Open Research Fund of Key Laboratory of Industrial Internet of Things & Networked Control, Ministry of Education under Grant 2023FF04; in part by the China National Key R&D Program under Grant 2021YFA1000500 and 2023YFB2904804; in part by the Zhejiang Provincial Natural Science Foundation of China under Grant LR22F010002; in part by the Zhejiang Provincial Science and Technology Plan Project under Grant 2024C01033; and in part by the Zhejiang University Global Partnership Fund. The associate editor coordinating the review of this article and approving it for publication was P. S. Bithas. *(Corresponding authors: Guofa Cai; Jiguang He.)*

Zhaokun Liang and Guofa Cai are with the School of Information Engineering, Guangdong University of Technology, Guangzhou 510006, China, and also with the Key Laboratory of Industrial Internet of Things and Networked Control, Ministry of Education, Chongqing University of Posts and Telecommunications, Chongqing 400065, China (e-mail: Liangzk98@163.com; caiguofa2006@gdut.edu.cn).

Jiguang He is with the School of Computing and Information Technology, Great Bay University, Dongguan 523000, China, and also with the Centre for Wireless Communications, University of Oulu, 90014 Oulu, Finland (e-mail: jiguang.he@gbu.edu.cn).

Georges Kaddoum is with the Electrical Engineering Department, École de Technologie Supérieure, University of Quebec, Montreal, QC H2L 2C4, Canada, and also with the Artificial Intelligence and Cyber Systems Research Centre, Lebanese American University, Beirut 797751, Lebanon (e-mail: georges.kaddoum@etsmtl.ca).

Chongwen Huang is with the College of Information Science and Electronic Engineering, Zhejiang University, Hangzhou 310027, China, and also with the Zhejiang Provincial Key Laboratory of Information Processing Communication and Network (IPCAN), Hangzhou 310027, China (e-mail: chongwenhuang@zju.edu.cn).

Digital Object Identifier 10.1109/TCOMM.2024.3511942

I. Introduction

TODAY, the Internet of Things (IoT) is extensively used in several important areas, such as autonomous driving, smart cities, environmental monitoring, satellite communication [1]. IoT applications frequently require long-range transmission and low-energy consumption [2]. To meet this need, low-power wide-area (LPWA) network technologies have been designed and widely applied in IoT applications. LoRa technology, one of the frontrunners in the emerging LPWA networks that is based on the chirp spread spectrum (CSS) modulation, supports low-energy consumption, reliable, and remote communication [2], [3]. An important benefit of the LoRa technology is that is governed by the spreading factor (SF), which affects the data rate and the communication range. In particular, a larger SF will increase the range and robustness, but will also lead to a very long transmission time. Unfortunately, despite the use of a large SF, long distance transmissions under complex wireless environments will bring more severe fading and interference, resulting in degraded transmission quality [4]. To improve the performance of the LoRa system, multiple-input multiple-output (MIMO) was introduced in [5], and some optimization problems for LoRa networks were formulated and solved in [6]. In addition, considering that a relay can also improve the system performance, another effective method to address signal attenuation is introducing cooperative communication into the LoRa system [7].

In recent years, reconfigurable intelligent surfaces (RISs) have emerged as another viable scheme owing to their ability to radio wave propagation without consuming energy and introducing additional noise [8], [9], [10], [11]. Specifically, RIS consists of inexpensive, intelligent, and virtually passive reflective elements that can be programmed and controlled by the RIS controller, thus enabling the reflection of the incident signal towards any desired direction [8]. Moreover, the space-feed mechanism of RISs avoids excessive power loss caused by large feed networks of phased arrays. Therefore, compared to MIMO and relay deployments, the use of RIS requires extremely low-power consumption and cost-effective hardware implementation [12]. To achieve the adjustment of incident signal, the phase shifts of the RIS reflecting

0090-6778 © 2024 IEEE. All rights reserved, including rights for text and data mining, and training of artificial intelligence and similar technologies. Personal use is permitted, but republication/redistribution requires IEEE permission.
See https://www.ieee.org/publications/rights/index.html for more information.
Authorized licensed use limited to: Universidad Federal de Pernambuco. Downloaded on July 29,2025 at 01:33:53 UTC from IEEE Xplore. Restrictions apply.

elements are configure d so that to control the directionality of the scattered signal beam. As a result, the signal reflected from RIS can be constructively added at the receiver, thus considerable boosting the strength of target signal. Due to these characteristics, RIS is considered as a key technology for future wireless communication systems.

To date, single-RIS-aided systems have been extensively studied in the literatures [11], [13], [14], [15]. In [11], using the central limit theorem (CLT) under Nakagami-m fading channels, the authors considered two phase configurations, i.e., random and coherent phase shifts, to analyze the outage probability and bit error rate (BER). In another relevant study [13], the authors also used the CLT to study the coverage, and the delay outage rate in the presence of Rayleigh fading channels. The results of this study demonstrated that the RIS-aided system brings more performance gains than the relay system and conventional RIS-free system. Furthermore, in [14] and [15], the authors derived the asymptotic outage probability and average rate under Rician fading channels. Therefore, the combination of LoRa technology and RIS is a promising scheme to facilitate the synergy between date rate and transmission distance by smart control of the radio wave propagation. For instance, recently, a single-RIS-aided LoRa system was proposed to achieve better BER and throughput performance as compared with the conventional RIS-free LoRa system [16]. In such a system, RIS adopts blind transmission scheme to combine signals without considering the adjustment of the RIS phase shifts, which is against the background of RIS' intelligent control for the wireless propagation. Very recently, in [17], the authors adopted RIS' optimal phase shifts to combine the target signal to analyze the performance in LoRa systems with an interfering user. However, this work neglect the effect of large-scale fading, i.e., path loss, which is significant for performance of long-range wireless systems.

In the present study, we setup a more generic system and introduce multi-RIS into LoRa systems. In recent years, several literatures studied the performance of multi-RIS-aided wireless systems [18], [19], [20], [21]. In [18], the authors studied the outage probability and average sum rate of the RIS-assisted system. Specifically, the RIS with the highest instantaneous end-to-end (E2E) signal-to-noise ratio (SNR) was picked from multiple available RISs. In addition, the authors relied on the extreme value theory to derive the asymptotic sum rate. In [19], the authors presented exhaustive and opportunistic schemes in multi-RIS-aided systems to analyze the outage probability and ergodic capacity under Nakagami-m fading channels by using moment-matching approach. In [20], the authors investigated a distributed RIS-aided system to explore the outage probability and achievable rate bounds in closed form. In [21], the authors developed and investigated multi-RIS-aided systems for non-line-of-sight (NLoS) scenarios. However, while previous studies [18], [19], [20], [21] have attempted to analyze the performance of multi-RIS systems, RISs with continuous phase shifts and perfect channel state information (CSI) were considered. Yet, in fact, these assumptions are limited because RIS consists of digital circuits, and its phase shift should be discrete [22]. Another limitation of previous research is that the CSI is often outdated due to the user mobility and the time overhead required for channel estimation in practice [23].

Several previous studies have studied the performance of RIS-aided wireless systems under the outdated CSI in [22], [23], [24], and [25]. In [22] and [24], the authors studied the ergodic capacity and outage probability over Rayleigh fading channels. Particularly, the authors also modeled the discrete phase shifts of RIS and analyzed its effect on the system performance in [22]. In [23], the authors investigated the ergodic capacity based on the centralized deployment and distributed deployment over Nakagami-m fading channels. Moreover, some insights for the ergodic capacity was also obtained by utilizing some inequalities. In [25], the authors obtained the outage probability, average BER, and average capacity in closed form based on the developed cumulative distribution function (CDF). Based on the observations in the aforementioned studies, erroneous channels generated by the outdated CSI came to be considered as a part of the noise term. This entails that this part has no impact on the E2E channel coefficient. However, as suggested by Eq. (3) in [22], Eq. (6) in [23], and Eq. (4) in [25], the E2E channel coefficient encompasses the erroneous channels. Therefore, unlike in [22], [23], [24], and [25], in the present study, we model the E2E channel coefficient by considering the joint outdated channels and erroneous channels to analyze the performance of the multi-RIS-aided LoRa system. Furthermore, in reality, the estimated CSI is imperfect due to estimation errors generated by the limited accuracy of the channel estimation algorithm [26], [27], [28]. Accordingly, it is essential to investigate the impact of imperfect estimation CSI on the performance.

The main contributions of this paper are summarized as follows:

- In this paper, we propose a generalized model for a multi-RIS-aided LoRa system to resist fading. In such a system, RISs can be intelligently controlled, and non-coherent and coherent detections are considered. Specifically, the outdated CSI, the imperfection of estimated CSI, and the discrete phase shift of RISs are modeled in the proposed system and their impacts are thoroughly investigated.
- We adopt the moment-matching method to obtain the E2E channel coefficient of the joint outdated channels and erroneous channels over Nakagami-m fading. Moreover, we derive the BER, throughput, delay outage rate, and the achievable diversity order of the proposed system in closed form.
- We perform simulations to verify the accuracy of our analytical method and obtain some important insight. The results reveal that, although coherent detection outperforms non-coherent detection in the low SNR regime, due to the error floor caused by the erroneous channels, it performs worse than non-coherent detection in the high SNR regime. In addition, we find that better BER can be achieved with stronger correlation between outdated channels and actual channels, higher channel estimation accuracy, more quantization bits for discrete phase shift design of RISs, and more number of RIS reflecting elements. We further analyze the throughput and delay outage rate performance of the proposed system. The Results reveal that, in the presence of outdated CSI and estimation errors, the BER, throughput, and delay outage rate performance of the proposed system is still superior to baseline schemes because of its tremendous diversity gain.

Authorized licensed use limited to: Universidad Federal de Pernambuco. Downloaded on July 29,2025 at 01:33:53 UTC from IEEE Xplore. Restrictions apply.

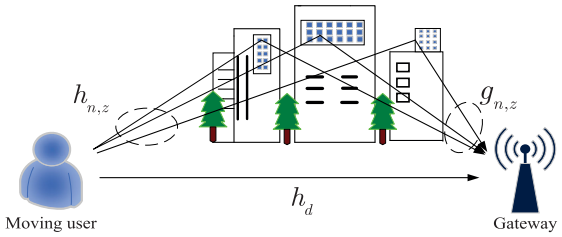

Fig. 1. The proposed multi-RIS-aided LoRa system model.

Mathematical Notation: $j = \sqrt{-1}$. $|\cdot|$ denotes absolute value operation. $\mathbb{C}^{p\times q}$ represents the space of $p \times q$ complex-valued matrices. $\Pr(\cdot)$ denotes the probability of an event. $f_R(\cdot)$ denotes the probability density function (PDF) of random variable (RV) R. $\mathrm{E}[\cdot]$ and $\mathrm{V}[\cdot]$ are the expectation and variance operators, respectively. $\mathcal{CN}(\mu,\sigma^2)$ and $\mathcal{N}(\mu,\sigma^2)$ are the complex Gaussian distribution and real Gaussian distribution with mean μ and variance σ^2, respectively. $*$ represents the complex conjugate operation, $D_a(\cdot)$ is the parabolic cylinder function, $J_d(\cdot)$ is the zeroth-order Bessel function of the first kind, $\gamma(\cdot)$ is the Gamma function, $\gamma(\cdot,\cdot)$ is the lower incomplete Gamma function, $\Gamma(\cdot,\cdot)$ is the the upper incomplete Gamma function, $Q(\cdot)$ is the Gaussian Q-function, and $\mathrm{erf}(\cdot)$ is the error function. Finally, $\Re(\cdot)$ and $\Im(\cdot)$ denote the real and imaginary operators, respectively.

II. System Model

Fig. 1 illustrates a single-input single-output (SISO) multi-RIS-aided LoRa system model that consists of a single-antenna moving LoRa user, a single-antenna gateway, and N RISs.[1] The N RISs are used to assist the communication between the LoRa node and the gateway. We assume that the n-th RIS has Z_n passive reflecting elements, and the RISs can be programmed by a controller to steer their beams toward the LoRa gateway. Therefore, we can stick to this assumption that the interference among the RISs can be ignored [9], [19], [23].

A. Channel Model

Let h_d denote the channel coefficient from the LoRa user to the gateway, $\mathbf{h}_n = [h_{n,1},\ldots,h_{n,z},\ldots,h_{n,Z_n}]^T \in \mathbb{C}^{Z_n\times 1}$, and $\mathbf{g}_n = [g_{n,1},\ldots,g_{n,z},\ldots,g_{n,Z_n}] \in \mathbb{C}^{1\times Z_n}$ denote the channel vectors from the user to the n-th RIS and from the n-th RIS to the gateway, respectively. We define $\mathbf{\Phi}_n = \mathrm{diag}\left(e^{j\kappa_{n,1}},\ldots,e^{j\kappa_{n,z}},\ldots,e^{j\kappa_{n,Z_n}}\right)$ as the phase shift matrix, where $\kappa_{n,z} \in [0,2\pi)$ is the phase shift of the z-th element of the n-th RIS. We consider the LoRa user mobility resulting in taking some time for feedback processing and channel estimation. Accordingly, it incurs outdated CSI. Specifically, h_d and $\mathbf{h}_n$ can be modeled, respectively, as

$$h_d = \varrho_d\tilde{h}_d + \sqrt{1-\varrho_d^2}e_d, \tag{1}$$

$$\mathbf{h}_n = \varrho_n\tilde{\mathbf{h}}_n + \sqrt{1-\varrho_n^2}\mathbf{e}_n, \tag{2}$$

where $0 \le \varrho_d \le 1$ is the correlation factor between the outdated channel $\tilde{h}_d$ and the actual channel h_d, while e_d is an erroneous channel independently distributed from $\tilde{h}_d$ following $\mathcal{CN}\left(0,\sigma_{h_d}^2\right)$. For Clarke's fading model, ϱ_d can be computed as $\varrho_d = J_d(2\pi f_d\tau_d)$, where f_d is the maximum Doppler shift generated by user movement, and τ_d is the estimated delay between the actual channel and the outdated channel [23]. Similarly, $\varrho_n = J_d(2\pi f_d\tau_n)\,(0 \le \varrho_n \le 1)$ is the n-th RIS correlation factor between the outdated channel $\tilde{\mathbf{h}}_n = [\tilde{h}_{n,1},\ldots,\tilde{h}_{n,z},\ldots,\tilde{h}_{n,Z_n}]^T \in \mathbb{C}^{Z_n\times 1}$ and the actual channel $\mathbf{h}_n$. Furthermore, $\mathbf{e}_n = [e_{n,1},\ldots,e_{n,z},\ldots,e_{n,Z_n}]^T \in \mathbb{C}^{Z_n\times 1}$ with $e_{n,z} \sim \mathcal{CN}\left(0,\sigma_{n,z}^2\right)$.

Since RISs are usually installed on the exterior wall of the building, the channels between them and the gateway vary relatively slow. Therefore, the RIS-gateway channels can be perfectly estimated by using previously proposed methods in [26] and [34]. However, in view of the mobility of the user, the user-RIS and user-gateway channels can rapidly change. Hence, the CSI of user-RIS and user-gateway becomes more tough to obtain as the user's position and environmental factors vary. Furthermore, since LoRa devices typically operate with low-complexity, the least-squares (LS) estimation algorithm is frequently adopted in LoRa systems [5]. If the channel is estimated with LS, the estimation error model of the user-RIS and user-gateway channels $\tilde{h}_d$ and $\tilde{h}_{n,z}$ can be reformulated as

$$\tilde{h}_d = \nu_d\hat{h}_d + \sqrt{1-\nu_d^2}\Delta h_d, \tag{3}$$

$$\tilde{h}_{n,z} = \nu_{n,z}\hat{h}_{n,z} + \sqrt{1-\nu_{n,z}^2}\Delta h_{n,z}, \tag{4}$$

respectively, where ν_d is the estimated correlation factor between $\hat{h}_d$ and $\tilde{h}_d$, and $\nu_{n,z}$ is the estimated correlation factor between $\hat{h}_{n,z}$ and $\tilde{h}_{n,z}$ [26], [35], [36]. In addition, $\hat{h}_d$ and $\hat{h}_{n,z}$ are the information obtained by the channel estimation technique, and Δh_d and $\Delta h_{n,z}$ represent the corresponding estimation error. Since $\hat{h}_d$ and $\hat{h}_{n,z}$ can be estimated by performing the same channel estimation method, we assume that the channel estimation error Δh_d and $\Delta h_{n,z}$ obey $\mathcal{CN}\left(0,\sigma_{\mathrm{err}}^2\right)$ [26], [28], i.e., $\Delta h_d \sim \mathcal{CN}\left(0,\sigma_{\mathrm{err}}^2\right)$ and $\Delta h_{n,z} \sim \mathcal{CN}\left(0,\sigma_{\mathrm{err}}^2\right)$. Specifically, σ_{err}^2 is dependent on the specific estimation method and the number of pilot symbols used. The estimated correlation factor can be set as $\nu = \nu_d = \nu_{n,z} = 1/\sqrt{1+\sigma_{\mathrm{err}}^2}$ [26]. Particularly, when $\sigma_{\mathrm{err}}^2 = 0$, we obtain $\nu = 1$ meaning perfect channel estimation.

By substituting Eq. (3) into Eq. (1), and Eq. (4) into Eq. (2), one can obtain

$$h_d = \varrho_d\nu\hat{h}_d + \varrho_d\bar{\nu}\Delta h_d + \bar{\varrho}_d e_d, \tag{5}$$

$$\mathbf{h}_n = \varrho_n\nu\hat{\mathbf{h}}_n + \varrho_n\bar{\nu}\Delta\mathbf{h}_n + \bar{\varrho}_n\mathbf{e}_n, \tag{6}$$

where $\bar{\nu} = \sqrt{1-\nu^2}$, $\bar{\varrho}_d = \sqrt{1-\varrho_d^2}$, $\bar{\varrho}_n = \sqrt{1-\varrho_n^2}$, $\hat{\mathbf{h}}_n = [\hat{h}_{n,1},\ldots,\hat{h}_{n,z},\ldots,\hat{h}_{n,Z_n}]^T \in \mathbb{C}^{Z_n\times 1}$, and $\Delta\mathbf{h}_n = [\Delta h_{n,1},\ldots,\Delta h_{n,z},\ldots,\Delta h_{n,Z_n}]^T \in \mathbb{C}^{Z_n\times 1}$.

In this study, we consider that all the uplinks undergo Nakagami-m fading, which is applicable for IoT applications, as we can easily switch between line-of-sight (LOS) and NLoS conditions by changing the parameter m ($m = 1$ represents Rayleigh fading with NLoS propagation condition, and a higher value of m represents better LoS propagation condition). Particularly, according to [11], Nakagami-m fading

[1]To simplify the analysis, this paper focuses on the analysis of multi-RIS-aided SISO LoRa systems where some significant factors of RISs are considered. Moreover, multi-antenna technology is a desirable solution, which is key technology for next-generation wireless systems. Recently, the performance of LoRa modulation can be significantly improved by using MIMO techniques [5], [29], [30]. In addition, the RIS-aided multi-antenna systems have been extensively studied recently [31], [32], [33]. Thus, it is interesting to introduce multiple-antenna technique to the proposed system in the future.

Authorized licensed use limited to: Universidad Federal de Pernambuco. Downloaded on July 29,2025 at 01:33:53 UTC from IEEE Xplore. Restrictions apply.

channels can be used to approximate Rician channels, where the relationship between parameter m and Rician factor ϖ can be obtained as $m = (1 - (\frac{\varpi}{1+\varpi})^2)^{-1}$. Therefore, we set $|\hat{h}_d| \sim \text{Nakagami}\,(m_d, 1)$, $|\hat{\mathbf{h}}_n| \sim \text{Nakagami}\,(m_{h_n}, 1)$, and $|\mathbf{g}_n| \sim \text{Nakagami}\,(m_{g_n}, 1)$, where m_d, m_{h_n} and m_{g_n} are shape parameters indicating the levels of fading severity.

Remark 1: Since channel estimation is essential for RIS-aided wireless communication systems in practice, in this paper, we comprehensively consider the impact of various important factors (i.e., outdated and imperfect CSI, and design of RIS discrete phase shifts) on the performance of the proposed system. In the following, we analyze the performance of LoRa detection based on these factors, which can provide some important insights for the application of RISs in LoRa systems.

B. The LoRa Transmitter

The LoRa user adopts the CSS technology to transmit information. A transmitted LoRa symbol is split into 2^δ samples within duration T_s, where $\delta \in \mathcal{F} = \{7, 8, 9, \ldots, 12\}$ denotes the spreading factor. Each LoRa sample occupies the time interval $T_c = \frac{1}{\Psi}$, where Ψ denotes the bandwidth.[2] A decimal symbol s is mapped to δ bits, where $s \in \mathcal{S} = \left\{0, 1, 2, \ldots, 2^{\delta-1}\right\}$. The signal frequency corresponding to s starts from $\frac{\Psi}{2^\delta}s$ and linearly increases until reaching $\frac{\Psi}{2}$. Afterwards, it returns to $-\frac{\Psi}{2}$, followed by a linear increase until the end of T_s. Therefore, a mathematical description of the symbol s is given by [3]

$$x_s(k) = e^{j2\pi\left(\frac{sk}{2^\delta} - \frac{k}{2} + \frac{k^2}{2^{\delta+1}}\right)}, k \in \mathcal{S}. \tag{7}$$

At the gateway, the received LoRa signal with the assistant of N RISs is given by

$$y_s(k) = \sqrt{P_s}\left(\varrho_d \Omega_d h_d + \sum_{n=1}^{N} \varrho_n \mathbf{g}_n \mathbf{\Omega}_n \mathbf{\Phi}_n \mathbf{h}_n\right) x_s(k) + \eta(k), \tag{8}$$

where P_s is the transmit power, and $\eta(k)$ is the complex additive white Gaussian noise (AWGN) following $\mathcal{CN}(0, N_0)$. We define $\Omega_d = \sqrt{d_{h_d}^{-\varepsilon_d}}$ as the path loss of the direct link, where d_{h_d} denotes the distance from the LoRa user to the gateway, and ε_{h_d} is the path loss exponent. In addition, we define $\mathbf{\Omega}_n = \text{diag}\,(\Omega_{n,1}, \ldots, \Omega_{n,z}, \ldots, \Omega_{n,Z_n})$ as the n-RIS path loss matrix. In this study, the far-field regime is assumed, thus all elements from the same RIS have the same path loss, i.e., $\Omega_{n,z} = \Omega_n = \sqrt{d_{h_n}^{-\varepsilon_{h_n}} d_{g_n}^{-\varepsilon_{g_n}}}, \forall z$, where d_{h_n} and d_{g_n} are the distances from the LoRa user to the n-th RIS, and from the n-th RIS to the gateway, respectively, and ε_{h_n} and ε_{g_n} are the corresponding path loss exponents. Due to the associated feedback delay and the user mobility, the estimated channel may frequently be imperfect and outdated. By substituting Eqs. (5) and (6) into Eq. (8), we can rewrite the received signal as

$$\begin{aligned} y_s(k) = &\underbrace{\sqrt{P_s}\left(\varrho_d \nu \Omega_d \hat{h}_d + \sum_{n=1}^{N} \varrho_n \nu \mathbf{g}_n \mathbf{\Omega}_n \mathbf{\Phi}_n \hat{\mathbf{h}}_n\right) x_s(k)}_{\text{Desired Signal}} \\ &+ \underbrace{\sqrt{P_s}\left(\varrho_d \bar{\nu} \Omega_d \Delta h_d + \sum_{n=1}^{N} \varrho_n \bar{\nu} \mathbf{g_n} \mathbf{\Omega}_n \mathbf{\Phi}_n \Delta \mathbf{h}_n\right) x_s(k)}_{\text{Signal with estimated error channels}} \\ &+ \underbrace{\sqrt{P_s}\left(\bar{\varrho}_d \Omega_d e_d + \sum_{n=1}^{N} \bar{\varrho}_n \mathbf{g}_n \mathbf{\Omega}_n \mathbf{\Phi}_n \mathbf{e}_n\right) x_s(k)}_{\text{Signal with outdated error channels}} + \eta(k). \end{aligned} \tag{9}$$

To maximize the received power of the desired signal, the optimal phase shifts can be designed as $\kappa_{n,z} = \lambda_{n,z} + \psi_{n,z} - \phi_d + \theta_{n,z}$, $\forall n, \forall z$ [18], [19], [23], where ϕ_d, $\lambda_{n,z}$, and $\psi_{n,z}$ are the phases of $\hat{h}_d$, $\hat{h}_{n,z}$ and $g_{n,z}$, respectively. In other words, the phase shifts of RISs are associated with the phases of $\hat{h}_d$, $\hat{h}_{n,z}$, and $g_{n,z}$. In addition, due to the mobility of the user and imperfect channel estimation, there may be errors while estimating the direct as well as user-RIS channel coefficients. However, the phase shifts of RISs are not matched with the erroneous channels [26], [28]. Moreover, in practice, the implementation of phase shifts of the RISs mostly depends on electronic components such as diodes and field-effect transistors [8]. Considering discrete phase shifts, let p_n denote the number of quantization bits and 2^{p_n} denote the number of discrete phase shifts for the n-th RIS. Then, the optimal phase shifts of the n-th RIS can be obtained from the closest discrete value from the set $\mathcal{I}_n = \{2\lambda\pi/2^{p_n}\}, \lambda \in \{0, 1, \ldots, 2^{p_n} - 1\}$ [19]. Therefore, the limitation of the digital circuit composition of RIS generates phase quantization errors. Let $\theta_{n,z} \sim \mathcal{U}(-\pi/2^{p_n}, \pi/2^{p_n})$ be the quantization error of the phase shift of the z-th reflecting element of the n-th RIS with p_n quantization bits. Hence, Eq. (9) can be re-expressed as[3]

$$\begin{aligned} y_s(k) = &\underbrace{\sqrt{P_s}\left(\varrho_d \nu \Omega_d \left|\hat{h}_d\right| + \sum_{n=1}^{N}\sum_{z=1}^{Z_n} \varrho_n \nu \Omega_n X_{n,z} e^{j\theta_{n,z}}\right) e^{-\phi_d} x_s(k)}_{\text{Desired signal with optimal phase shifts}} \\ &+ \sqrt{P_s}\left(\varrho_d \bar{\nu} \Omega_d \Delta h_d + \sum_{n=1}^{N} \varrho_n \bar{\nu} \mathbf{g}_n \mathbf{\Omega}_n \mathbf{\Phi}_n \Delta \mathbf{h}_n\right) x_s(k) \\ &+ \sqrt{P_s}\left(\bar{\varrho}_d \Omega_d e_d + \sum_{n=1}^{N} \bar{\varrho}_n \mathbf{\Phi}_n \mathbf{\Omega}_n \mathbf{\Phi}_n \mathbf{e}_n\right) x_s(k) + \eta(k), \end{aligned} \tag{10}$$

where $X_{n,z} = |\hat{h}_{n,z}||g_{n,z}|$.

Remark 2: In conventional RIS-free LoRa systems, the synchronization implementation requires preamble symbols in LoRa packets, while for the proposed multi-RIS-aided LoRa system, the preamble symbols are utilized not only for synchronization, but also for estimation of a cascade of RIS channels. Therefore, the LoRa packet structure does not require to be adapted, and the typically utilized LoRa MAC protocol remains applicable [5], [38].

[2] According to [37], the sampling frequency is set as the value of bandwidth for the following LoRa demodulation.

[3] Every LoRa packet starts with a preamble usually containing 12.25 symbols, followed by payload symbols [39]. The preamble symbols are utilized for channel estimation to obtain CSI. Thus, in practice, RIS controllers can be connected via a high-speed backhaul link to synchronize the phase-shift configuration by using the obtained CSI [19], [40], [41]. During each symbol transmission interval, the gateway can receive the improved payload symbol by combining the direct link and additional RIS-reflected propagation paths.

Authorized licensed use limited to: Universidad Federal de Pernambuco. Downloaded on July 29,2025 at 01:33:53 UTC from IEEE Xplore. Restrictions apply.

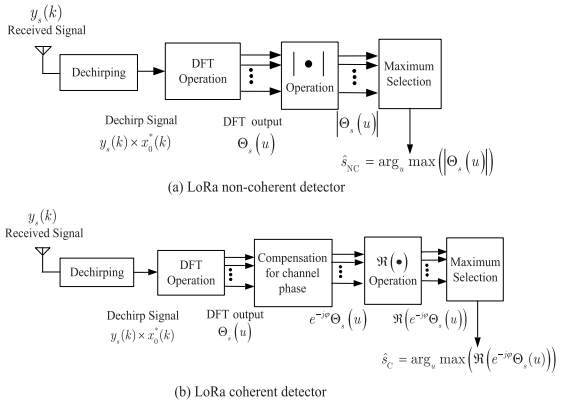

Fig. 2. Block diagram of the LoRa detectors.

C. The Gateway Receiver

To recover the transmit information, the received signal at the gateway must be demodulated. Fig. 2 shows the the detector structure of the LoRa system, where both non-coherent and coherent detections are employed. The first task is dechirping. The dechirped signal can be obtained from the product of the received signal and the complex conjugate of the basic signal $x_0(k)$, given by

$$\tilde{y}_s(k) = y_s(k) \times x_0^*(k) = \sqrt{P_s} H e^{j2\pi \times \frac{sk}{2^\delta}} + \tilde{\eta}(k), \quad (11)$$

where

$$\begin{aligned} H = &\left(\varrho_d \nu \Omega_d \left| \hat{h}_d \right| + \sum_{n=1}^{N} \sum_{z=1}^{Z_n} \varrho_n \nu \Omega_n X_{n,z} e^{j\theta_{n,z}} \right) e^{-\phi_d} \\ &+ \varrho_d \bar{\nu} \Omega_d \Delta h_d + \sum_{n=1}^{N} \varrho_n \bar{\nu} \mathbf{g}_n \mathbf{\Omega}_n \mathbf{\Phi}_n \Delta \mathbf{h}_n \\ &+ \bar{\varrho}_d \Omega_d e_d + \sum_{n=1}^{N} \bar{\varrho}_n \mathbf{g}_n \mathbf{\Omega}_n \mathbf{\Phi}_n \mathbf{e}_n, \end{aligned} \quad (12)$$

and $\tilde{\eta}(k) = \eta(k) x_0^*(k)$ is also the complex AWGN. Next, the discrete Fourier transform (DFT) is conducted for the resultant multiplication [42]. The DFT output is calculated as

$$\begin{aligned} \Theta_s(u) &= \mathrm{DFT}\left(\tilde{y}_s(k)\right) \\ &= \sum_{k=0}^{2^{\delta-1}} \sqrt{P_s} H e^{j\frac{2\pi(s-u)k}{2^\delta}} + \underbrace{\sum_{k=0}^{2^{\delta-1}} \tilde{\eta}(k) e^{-j\frac{2\pi u k}{2^\delta}}}_{Z(u)} \\ &= \begin{cases} \sqrt{P_s} 2^\delta H + Z(u), & u = s \\ Z(u), & u \neq s, \end{cases} \end{aligned} \quad (13)$$

where $u \in \mathcal{S}$ is the possible symbol, and $Z(u) \sim \mathcal{CN}\left(0, 2^\delta N_0\right)$.

In non-coherent detection, the frequency index $\hat{s}$ with the largest magnitude of $\Theta_s(u)$ is selected [4], which is expressed as

$$\hat{s}_{\mathrm{NC}} = \arg_u \max\left(|\Theta_s(u)|\right)$$

$$= \begin{cases} \left| \sqrt{P_s} H 2^\delta + Z(u) \right|, & u = s \\ |Z(u)|, & u \neq s. \end{cases} \quad (14)$$

Coherent detection is that the outdated channel phase shift must be compensated. Therefore, the compensated phase is $\varphi = -\phi_d$. Then, the coherent detection is to select the frequency index $\hat{s}$ with the maximum real part value of $e^{-j\varphi}\Theta_s(u)$ [3], expressed as

$$\begin{aligned} \hat{s}_{\mathrm{C}} &= \arg_u \max\left(\Re\left(e^{-j\varphi}\Theta_s(u)\right)\right) \\ &= \begin{cases} \Re\left(\sqrt{P_s} H 2^\delta e^{-j\varphi} + e^{-j\varphi} Z(u)\right), & u = s, \\ \Re\left(Z(u)\right), & u \neq s. \end{cases} \end{aligned} \quad (15)$$

According to Eq. (13), when the LoRa symbol s is dechirped, all signal energy is concentrated at the s-th frequency bin, while all the remaining $2^\delta - 1$ bins consist of only noise samples.

D. Discussion of Erroneous Channels

The performance of RIS-aided systems with outdated CSI has been studied in the literature [22], [23], [24], [25]. Yet, previous studies treated the signal with erroneous channels as part of the noise term. This appears to be less rational in LoRa systems, as according to Eq. (12), the E2E channel coefficient H is the sum of both the outdated and erroneous channels, while only complex AWGN acts as a noise term. To clarify this point, we use the LoRa detection as an example to elaborate this problem.

On the one hand, following Eqs. (14) and (15), the received energy for transmit symbol s depends on the value of H, which consists of the sum of the outdated channels and erroneous channels. Hence, the signal with erroneous channels also carries useful information. Furthermore, a more specific example is shown in Fig. 3 (a) and (b), where $\varrho_d = \varrho_n = 0$, $Z_n = 20$, $\forall n$, the transmit decimal symbol $s = 100$, and other specific parameters are specified in Section IV. Fig. 3 (a) and (b) shows that, although there are only erroneous channels (i.e., the CSI is completely fresh), the peak location is the same for non-coherent and coherent detections, which occurs in the 100-th frequency bin. Then, the detectors can correctly select the maximum value and then recover the transmit information. This confirms that the signal of erroneous channels participate in the detection process, rather than are mere noise.

Following the above analysis, we note that coherent detector is to select the maximum value of $\Re\left(\sqrt{P_s} 2^\delta H e^{-j\varphi} + e^{-j\varphi} Z(u)\right)$ for all possible symbols after the DFT. We observe that the correctness of coherent detection mainly depends on the channel coefficient $\Re\left(He^{-j\varphi}\right)$. Yet, due to the presence of erroneous channels, coherent detector cannot fully compensate for channel phase, which deteriorates its detection performance. In what follows, we use some mathematical methods to illustrate this problem. After the compensation for the phase shift of outdated channels, we obtain the fading coefficient for the transmit symbol, expressed as $He^{-j\varphi} = H_1 + H_2 + H_3$, where

$$H_1 = \varrho_d \nu \Omega_d |\hat{h}_d| + \sum_{n=1}^{N} \sum_{z=1}^{Z_n} \varrho_n \nu \Omega_{n,z} X_{n,z} e^{j\theta_{n,z}}, \quad (16)$$

Authorized licensed use limited to: Universidad Federal de Pernambuco. Downloaded on July 29,2025 at 01:33:53 UTC from IEEE Xplore. Restrictions apply.

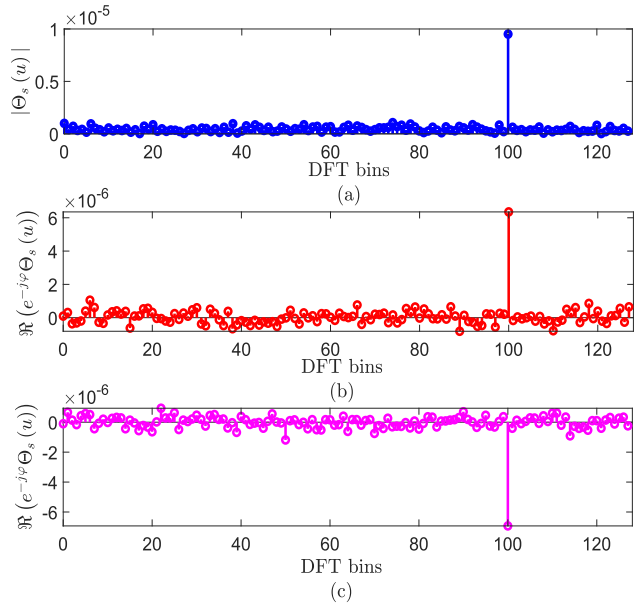

Fig. 3. Illustration of correct detection for non-coherent detector (a), coherent detector (b), and erroneous detection for coherent detector (c), where $\varrho_d = \varrho_n = 0$, $Z_n = 20$, $\forall n$, and the transmit decimal symbol $s = 100$.

$$H_2 = \left(\varrho_d \bar{\nu} \Omega_d \Delta h_d + \sum_{n=1}^{N} \varrho_n \bar{\nu} \mathbf{g}_n \mathbf{\Omega}_n \mathbf{\Phi}_n \Delta \mathbf{h}_n \right) e^{-j\varphi}, \quad (17)$$

and

$$H_3 = \left(\bar{\varrho}_d \Omega_d e_d + \sum_{n=1}^{N} \bar{\varrho}_n \mathbf{g}_n \mathbf{\Omega}_n \mathbf{\Phi}_n \mathbf{e}_n \right) e^{-j\varphi}. \quad (18)$$

Since the fading coefficient can be further expressed as $He^{-j\varphi} = |H| e^{-j\varphi_h}$ with $|H| = \sqrt{\left[\Re\left(H_1 + H_2 + H_3\right)\right]^2 + \left[\Im\left(H_1 + H_2 + H_3\right)\right]^2}$ and $\varphi_h = \arctan\left(-\frac{\Im(H_1+H_2+H_3)}{\Re(H_1+H_2+H_3)}\right)$, we have $\Re\left(He^{-j\varphi}\right) = |H| \cos\left(\varphi_h\right)$. If $-\pi < \varphi_h \leq -\frac{\pi}{2}$ and $\frac{\pi}{2} < \varphi_h \leq \pi$ occur in simulation, $\Re\left(He^{-j\varphi}\right)$ becomes a negative number, resulting in a minimum value at $u = s$, as shown in Fig. 3 (c). Therefore, selecting the maximum value of $\Re\left(\sqrt{P_s} H 2^{\delta} e^{-j\varphi} + e^{-j\varphi} Z\left(u\right)\right)$ detects the erroneous symbol, thereby degrading the BER performance of coherent detection.

III. Performance Analysis

A. BER Analysis

1) Noncoherent Detection: According to Eqs. (13) and (14), a symbol error occurs in LoRa non-coherent detection when

$$\max_{u \in \mathcal{S}, u \neq m} \left(\left(|\Theta_s(u)| \right) > |\Theta_s(u \mid u = s)| \right), \quad (19)$$

where $\max_{u \in \mathbf{S}, u \neq m} \left(|\Theta_s(u)| \right)$ approximates a constant $\sqrt{N_0 \Lambda_{2^{\delta}-1}}$ related to δ in [4], as it shows a low coefficient of variation. Accordingly, the conditional symbol error rate (SER) probability for non-coherent detection corresponding to H can be calculated as

$$P_{s|H}^{\mathrm{NC}} \approx \Pr\left(\sqrt{N_0 \Lambda_{2^{\delta}-1}} > |\Theta_s(u \mid u = s)| \right). \quad (20)$$

In Eq. (20), $\Theta_s(u \mid u = s) = \sqrt{P_s} 2^{\delta} |H| e^{-j\vartheta} + Z\left(u\right)$ follows a complex Gaussian distribution, where ϑ is the phase of $|H|$. Hence, $\Theta_s(u \mid u = s)$ can be further expressed as

$$\Theta_s(u \mid u = s) \sim \mathcal{CN}\left(\sqrt{P_s} 2^{\delta} |H| \cos\left(\vartheta\right) - j \sqrt{P_s} 2^{\delta} |H| \sin\left(\vartheta\right), 2^{\delta} N_0 \right). \quad (21)$$

Using the properties of the complex Gasussian distribution, $|\Theta_s(u \mid u = s)|$ obeys a Rician distribution with the shape parameter $\frac{P_s |H|^2 2^{\delta}}{N_0}$. In LoRa, due to $\delta \geq 7$, we have a relative high shape parameter [4]. Thus, for large shape parameters, a Rician distribution can be approximated as a Gaussian distribution with mean $\sqrt{2^{\delta} P_s} |H|$ and variance $N_0/2$ [4], [7]. It should be noted that $|H|$ can be temporarily treated as a constant in conditional SER expression. Accordingly, Eq. (20) can be computed as

$$P_{s||H|}^{\mathrm{NC}} \approx Q\left(\frac{\sqrt{2^{\delta} P_s} |H| - \sqrt{N_0 \Lambda_{2^{\delta}-1}}}{\sqrt{N_0/2}} \right). \quad (22)$$

Furthermore, the conditional BER P_b^{NC} can be expressed as

$$P_{b||H|}^{\mathrm{NC}} \approx 0.5 \times Q\left(\sqrt{2 \times 2^{\delta} \bar{\rho} |H|^2} - \sqrt{2\Lambda_{2^{\delta}-1}} \right), \quad (23)$$

where $\bar{\rho} = \frac{P_s}{N_0}$ denotes the average SNR, which increases with an increase of the transmit power. Hence, P_b^{NC} is computed as

$$P_b^{\mathrm{NC}} \approx 0.5 \times \int_0^{\infty} Q\left(\sqrt{2^{\delta+1} \bar{\rho} x} - \sqrt{2\Lambda_{2^{\delta}-1}} \right) f_{|H|^2}\left(x\right) dx. \quad (24)$$

Since $|H|^2$ includes a series of outdated and erroneous channels, it is challenging to directly obtain the PDF of $|H|^2$. To circumvent this issue, we use the moment-matching approach to approximate $|H|^2$ to a Gamma distribution in Theorem 1. This is because the Gamma distribution is a Type-III Pearson distribution extensively applied in matching distribution for positive RVs by obtaining their first and second moments [43].

Theorem 1: The PDF of $|H|^2$ can be approximated to the Gamma distribution:

$$f_{|H|^2}\left(x\right) \approx \frac{\beta^{\alpha}}{\gamma(\alpha)} x^{\alpha-1} e^{-\beta x}, x \geq 0, \quad (25)$$

where α and β are the scale and shape estimators, respectively, expressed as

$$\alpha = \frac{\left(\mathrm{E}[|H|^2]\right)^2}{\mathrm{E}[|H|^4] - \left(\mathrm{E}[|H|^2]\right)^2}, \beta = \frac{\mathrm{E}[|H|^2]}{\mathrm{E}[|H|^4] - \left(\mathrm{E}[|H|^2]\right)^2}, \quad (26)$$

where $\mathrm{E}[|H|^2]$ and $\mathrm{E}[|H|^4]$ are given in Eqs. (49) and (67), respectively. *Proof:* The proof is provided in Appendix A. □

Accordingly, the BER for non-coherent detection can be computed as

$$P_b^{\mathrm{NC}} \approx 0.5 \int_0^{\infty} Q\left(\sqrt{2^{\delta+1} \bar{\rho} x} - \sqrt{2\Lambda_{2^{\delta}-1}} \right) \times \frac{\beta^{\alpha} e^{-\beta x}}{\gamma(\alpha)} x^{\alpha-1} dx.$$

Authorized licensed use limited to: Universidad Federal de Pernambuco. Downloaded on July 29,2025 at 01:33:53 UTC from IEEE Xplore. Restrictions apply.

(27)

Then, utilizing integration by parts, Eq. (27) can be calculated as

$$\begin{aligned} P_b^{\mathrm{NC}} &\approx 0.5 \times \sum_{\omega=0}^{\alpha-1} \frac{e^{-\beta x} x^{\alpha-1-\omega}}{\beta^{\omega+1}\gamma(\alpha-\omega)} x^{\alpha-1-\omega} Q\left(\sqrt{2B}-A\right)|_0^{\infty} \\ &- \sum_{\omega=0}^{\alpha-1} \frac{\beta^{\alpha-\omega-1}\sqrt{B}}{\gamma(\alpha-\omega)\sqrt{32\pi}} \int_0^{\infty} e^{-\beta x-\frac{1}{2}\left(\sqrt{B}x-A\right)^2} x^{\alpha-\omega-\frac{3}{2}} dx, \end{aligned} \tag{28}$$

where $A = \sqrt{2\Lambda_{2^\delta-1}}$, and $B = 2^{\delta+1}\bar{\rho}$. Since α is not necessarily obtained as an integer, we approximate it to the nearest integer of α in the summation operation.

Assigning $t = \sqrt{x}$ and using Eqs. (3.462.1) and (9.240) in [44] along with some mathematical manipulations, P_b^{NC} can be computed as

$$\begin{aligned} P_b^{\mathrm{NC}} &\approx 0.5 \times Q(-A) - \sqrt{\frac{B}{8\pi}} \beta^{\alpha} e^{-\frac{1}{2}A^2 + \frac{A^2 B}{4(B+2\beta)}} \\ &\times D_{-2\alpha+2\omega+1}\left(\frac{-A\sqrt{B}}{\sqrt{2\beta+B}}\right) \\ &\times \sum_{\omega=0}^{\alpha-1} \frac{(2\beta+B)^{-\alpha-\omega+\frac{1}{2}}}{\beta^{\omega+1}\gamma(\alpha-\omega)} \gamma(2\alpha-2\omega-1). \end{aligned} \tag{29}$$

Remark 3: When $P_s \to \infty$, we obtain $B \to \infty$, and Eq. (29) can be approximated as

$$P_b^{\mathrm{NC}} \approx 0.5 \times Q(-A) - \sqrt{\frac{1}{8\pi}} e^{-\frac{A^2}{4}} D_{-1}(-A). \tag{30}$$

Using Eq. (9.254.1) in [44], one has $D_{-1}(-A) = e^{\frac{A^2}{4}}\sqrt{\frac{\pi}{2}}[1-\mathrm{erf}(\frac{-A}{\sqrt{2}})]$. Using the relationship $\mathrm{erf}(x) = 1 - 2Q\left(\sqrt{2}x\right)$, $D_{-1}(-A)$ can be further computed as $D_{-1}(-A) = \sqrt{2\pi}e^{\frac{A^2}{4}}Q(-A)$. Finally, substituting it into Eq. (30), we obtain $P_b^{\mathrm{NC}} \approx 0$, which means that, in the large SNR regime (i.e., the transmit power is sufficiently high), the BER of non-coherent detection approximates zero.

2) Coherent Detection: According to Eqs. (13) and (15), a symbol error occurs in LoRa coherent detection when

$$\max_{u\in\mathbf{S}, u\neq m} \Re\left(e^{-j\varphi}\Theta_s(u)\right) > \Re\left(e^{-j\varphi}\Theta_s(u \mid u=s)\right), \tag{31}$$

where $\max_{u\in\mathbf{S},u\neq m}\left(\Re\left(e^{-j\varphi}\Theta_s(u)\right)\right)$ can be approximated as a Gassuian random variable with λ_2 mean and variance σ_5^2 [42], where

$$\lambda_2 = \sqrt{\frac{2^\delta N_0}{2}}(1.161 + 0.2074\delta), \tag{32}$$

$$\sigma_5^2 = \frac{2^\delta N_0}{2}(0.2775 - 0.0153\delta). \tag{33}$$

Hence, the conditional symbol error probability for coherent detection corresponding to H is approximated as

$$P_b^{\mathrm{C}} \approx \Pr\left(\max_{u\in\mathcal{S}, u\neq m} \Re\left(e^{-j\varphi}\Theta_s(u)\right) > \Re\left(e^{-j\varphi}\Theta_s(u|u=s)\right)\right), \tag{34}$$

where $\Re\left(e^{-j\varphi}\Theta_s(u \mid u=s)\right) = \Re\left(\sqrt{P_s}H2^\delta e^{-j\varphi} + Z(u)\right)$.

Similarly, since $\Re(He^{-j\varphi})$ is the sum of the random variables about the fading channels, the derivation of closed-form expressions for its PDF becomes intractable. Accordingly, to circumvent this problem, we obtain the approximate distribution of $\Re(He^{-j\varphi})$ by relying on moment-matching method. Of note, however, it is not appropriate to approximate $\Re(He^{-j\varphi})$ as a Gamma distribution like $|H|^2$, as $|H|^2$ is greater than or equal to 0, which is suitable for being approximated as a Gamma distribution, while $\Re(He^{-j\varphi})$ is a random variable that takes values from $-\infty$ to ∞. Following [20], the Gaussian distribution can also approximate the true distributions for a series of RVs with a high-accuracy by obtaining the mean and variance. Hence, we can approximate $\Re(He^{-j\varphi})$ as a Gaussian distribution.

Theorem 2: $\Re(He^{-j\varphi})$ can be approximated as the Gaussian distribution, which is fitting by two parameters λ_3 and σ_6^2, i.e., $\Re\left(He^{-j\varphi}\right) \sim \mathcal{N}\left(\lambda_3, \sigma_6^2\right)$, where λ_3 and σ_6^2 are deduced in the following proof.

Proof: The proof is provided in Appendix B. □

Using the property of the Gaussian distribution, we obtain $\Re(\sqrt{P_s}2^\delta He^{-j\varphi} + Z(u)e^{-j\varphi}) \sim \mathcal{N}(\sqrt{P_s}2^\delta\lambda_3, P_s 2^{2\delta}\sigma_6^2 + \frac{2^\delta N_0}{2})$. According to Eqs. (31) and (34), the BER performance for coherent detection is attributed to the probabilistic comparison between two Gaussian random variables, computed as

$$\begin{aligned} P_b^{\mathrm{C}} &\approx \int_0^{\infty} \frac{1/2\sqrt{2\pi}}{\sqrt{P_s 2^{2\delta}\sigma_6^2 + \sigma_5^2 + \frac{2^\delta N_0}{2}}} \times e^{\frac{\left[x-\left(\sqrt{P_s}2^\delta\lambda_3-\lambda_2\right)^2\right]}{2\left(P_s 2^{2\delta}\sigma_6^2+\sigma_5^2+\frac{2^\delta N_0}{2}\right)}} dx \\ &\approx \frac{1}{2}Q\left(\frac{\sqrt{P_s 2^\delta}\lambda_3 - \frac{1}{\sqrt{2^\delta}}\lambda_2}{\sqrt{P_s 2^\delta\sigma_6^2 + \frac{1}{2^\delta}\sigma_5^2 + \frac{N_0}{2}}}\right). \end{aligned} \tag{35}$$

Remark 4: When $P_s \to \infty$, meaning that the SNR is sufficiently large, we obtain $P_b^{\mathrm{C}} \approx \frac{1}{2}Q\left(\frac{\lambda_3}{\sigma_6}\right)$, which shows that the BER for coherent detection encounters a error floor related only to the two channel estimators λ_3 and σ_6.

B. Throughput

In LoRa systems, a important performance metric is the throughput, which is defined as the amount of bits that correctly detected by the gateway per second. Hence, the throughput for the proposed system is computed as

$$R = W \times \delta \times (1 - P_E)/T_t, \tag{36}$$

where W is the amount of symbols in a physical layer packet, and $T_t = T_s \times W$ denotes the total transmission period per packet. Furthermore, P_E is error rate for this packet, which can be expressed as

$$P_E = 1 - (1 - P_s^{\upsilon})^W. \tag{37}$$

In Eq. (37), $P_s^{\upsilon} = \frac{2^\delta - 1}{2^\delta - 1} P_b^{\upsilon}$ is the symbol error of the proposed system, where $\upsilon \in \{\mathrm{NC}, \mathrm{C}\}$ with NC and C denoting non-coherent detection and coherent detection, respectively.

Authorized licensed use limited to: Universidad Federal de Pernambuco. Downloaded on July 29,2025 at 01:33:53 UTC from IEEE Xplore. Restrictions apply.

In addition, in LoRa systems, there are W symbols in one physical layer packet, expressed as

$$W = W_{\text{pre}} + 8 + L_\delta \times (\Upsilon + 4). \tag{38}$$

In Eq. (38), $W_{\text{pre}} = 4.25 + W_{\text{pro}}$ is the number of preamble symbols, where W_{pro} is the number of programmable symbols. In addition, $\Upsilon \in \{1, 2, 3, 4\}$ is coding rate. Meanwhile, L_δ is calculated as

$$L_\delta = \max\left(\left\lceil \frac{8W_{\text{m}} - 4\delta + 28 + 16C - 20I}{4 \times (\delta - 2E)} \right\rceil, 0\right), \tag{39}$$

where $\lceil \cdot \rceil$ is the ceiling function, W_{m} is the number of bytes in MAC layer payload, C is set to 1 by default in LoRaWAN to achieve cyclic redundancy check, and $I \in \{0, 1\}$ is the header feature flag, which is set to 1 to configure implicit mode and 0 when the header is explicit. Moreover, $E = 1$ means that a data optimization feature in LoRa is enabled.

C. Delay Outage Rate

Delay outage rate is an important performance metric that can effectively indicate communication latency of a wireless communication system. Delay outage rate of the proposed system is defined as the probability that the time needed to successfully transmission for a packet exceeds a time threshold T_{th}. In practice, the threshold T_{th}, also refers to as time on air in LoRa systems, is the sum of the transmission time for the preamble and payload symbol [38], [45]. Therefore, T_{th} increases with an increase of the value of δ, defined as $T_{th} = W \times \frac{2^\delta}{\Psi}$ [45, Eq. (8)]. Accordingly, the delay outage rate is expressed as

$$P_{\text{DOR}} = \Pr\left(T_D > T_{th}\right), \tag{40}$$

where T_D is the required delivery time. In LoRa systems, T_D can be computed as $T_D = \frac{W \times \delta}{K_D}$, where $W \times \delta$ is the number of bits, and K_D is the actual rate of transmission. To address the delay outage rate in a closed-form, the Shannon capacity theorem is applied to obtain the performance bound for LoRa packets [46, Eq. (3)]. Accordingly, T_D can be computed as $T_D = \frac{W \times \delta}{\Psi \log_2\left(1 + \bar{\rho}|H|^2\right)}$.

Hence, Eq. (40) can be calculated as

$$P_{\text{DOR}} = \Pr\left(|H|^2 < \frac{2^{\frac{\delta}{2^\delta}} - 1}{\bar{\rho}}\right), \tag{41}$$

which indicates that the delay outage rate probability is the CDF of $|H|^2$. According to Theorem 1, $|H|^2 \sim \text{Gamma}(\alpha, \beta)$. The CDF of $|H|^2$ is obtained in [19], i.e., $F_{|H|^2}(x) = \frac{\gamma(\alpha, \beta x)}{\gamma(\alpha)}, x \geq 0$. In addition, since $\gamma(\kappa, x) + \Gamma(\kappa, x) = \gamma(\kappa)$, Eq. (41) can be calculated as

$$P_{\text{DOR}} \approx \frac{\gamma\left(\alpha, \beta \frac{2^{\frac{\delta}{2^\delta}} - 1}{\bar{\rho}}\right)}{\gamma(\alpha)} \approx 1 - \frac{1}{\gamma(\alpha)} \Gamma\left(\alpha, \beta \frac{2^{\frac{\delta}{2^\delta}} - 1}{\bar{\rho}}\right). \tag{42}$$

Utilizing $\Gamma(\kappa, x) = \Gamma(\kappa) e^{-x} \sum_{\chi=0}^{\kappa-1} \frac{1}{\chi!} x^\chi$, Eq. (42) can be rewritten as

$$P_{\text{DOR}} \approx 1 - e^{-\beta \times \frac{2^{\frac{\delta}{2^\delta}} - 1}{\bar{\rho}}} \sum_{\Delta=0}^{\alpha-1} \frac{1}{\Delta!} \left(\beta \frac{2^{\frac{\delta}{2^\delta}} - 1}{\bar{\rho}}\right)^\Delta. \tag{43}$$

For a large $\bar{\rho}$, using $1 - e^{-t} \sum_{\chi=0}^{\tau-1} \frac{x^\chi}{\chi!} \leq \frac{t^\tau}{\tau}$, Eq. (43) can be approximated as

$$P_{\text{DOR}} \approx 1 - \left[1 - \frac{1}{\alpha!} \left(\beta \frac{2^{\frac{\delta}{2^\delta}} - 1}{\bar{\rho}}\right)^\alpha\right] \approx \frac{1}{\alpha!} \left(\beta \frac{2^{\frac{\delta}{2^\delta}} - 1}{\bar{\rho}}\right)^\alpha. \tag{44}$$

Based on Eq. (44), diversity order of the proposed system can be computed as $G_p = -\lim_{\bar{\rho} \to \infty} \left[\frac{\log(P_{\text{DOR}})}{\log(\bar{\rho})}\right] = \alpha$. Accordingly, the diversity order of the proposed system depends on the Gamma estimator α. In fact, when CSI is available so as to configure the phase shifts of the RISs to maximize the received power of the desired signal, the value of α increases with an increase of the number of reflecting elements [19], [47].

Moreover, we present the diversity order of two baseline schemes, i.e., RIS-aided LoRa systems adopting blind transmission and RIS-free LoRa systems. The blind transmission scheme is that, when CSI is not available at the gateway, i.e., the phase shifts $\kappa_{n,z}$ is uniformly distributed in $[0, 2\pi]$, $\forall n, \forall z$. Diversity order of blind transmission scheme can be obtained in [11], expressed as $G_b = 1$. Therefore, diversity order of the blind scheme is always 1, i.e., independent to the number of reflecting elements and fading parameters. Conversely, when only the direct link exists, i.e., in RIS-free LoRa systems, delay outage rate is computed as $P^d_{\text{DOR}} = \Pr(|\hat{h}_d|^2 < \frac{2^{\frac{\delta}{2^\delta}} - 1}{\bar{\rho} \varrho_d^2 \Omega_d^2})$. Since $|\hat{h}_d| \sim \text{Nakagami}(m_d, 1)$, we obtain $|\hat{h}_d|^2 \sim \text{Gamma}(m_d, 1)$. Therefore, similar to the derivation of Eq. (41), the diversity order can be computed as $G_d = -\lim_{\bar{\rho} \to \infty} \left[\log\left(P^d_{\text{DOR}}\right) / \log\left(\bar{\rho}\right)\right] = m_d$, which is related to the fading coefficient of the direct link.

IV. Results and Discussions

In this section, we provide numerical results to verify the analytical framework of the proposed system. Unless stated otherwise, we set $\Psi = 125$ kHz, and the number of the RISs and Nakagami-m shape parameters are set as $N = 4$ and $m_d = m_{h_n} = m_{g_n} = 2$, respectively. Considering the urban environment, we set $d_{h_d} = 3000$ m, and the path loss exponents $\varepsilon_{h_d} = \varepsilon_{h_n} = \varepsilon_{g_n} = 2.65$ [48]. The variance of the Gaussian noise is computed as $N_0 = -174 + N_f + 10\log_{10}(\Psi)$, where $N_f = 6$ dB is the noise figure. For outdated parameters, we set $\sigma^2_{n,z} = \sigma^2_n = 0.6$, and $\varrho_d = \varrho_n = \varrho$, $\forall n$. We assume that each RIS adopts the same number of bits to quantify its phase shifts, i.e., $p_n = p$, $\forall n$, and has the same number of reflecting elements, i.e., $Z_n = Z$, $\forall n$. To satisfy the long-distance communication requirement, the positions of the LoRa user and the gateway are set to $(0, 0)$ and $(0, 3000)$, respectively. In addition, to mitigate the multiplicative path loss of the RISs, we assume that the RISs are deployed close to the gateway. The locations of the four RISs are set to $(2960, 10)$, $(2970, 10)$, $(2980, 10)$, $(2990, 10)$, respectively. Moreover, several parameters for LoRa packet are shown in Table I.

In Fig. 4, we validate the correctness of our developed analysis in Theorems 1 and 2. To this end, we plot the true and approximate distributions of $|H|^2$ and $\Re\left(He^{-j\varphi}\right)$, where $Z = 30$, $\varrho = 0.9$, $\sigma^2_{\text{err}} = 0.2$, and $p = 2$. The true distributions are generated through Monte Carlo simulations, and the

Authorized licensed use limited to: Universidad Federal de Pernambuco. Downloaded on July 29,2025 at 01:33:53 UTC from IEEE Xplore. Restrictions apply.

TABLE I
SOME PARAMETERS FOR LORA PACKET

W_{pre}	W_{m}	Υ	C	I	E
12.25	33	1	1	0	0

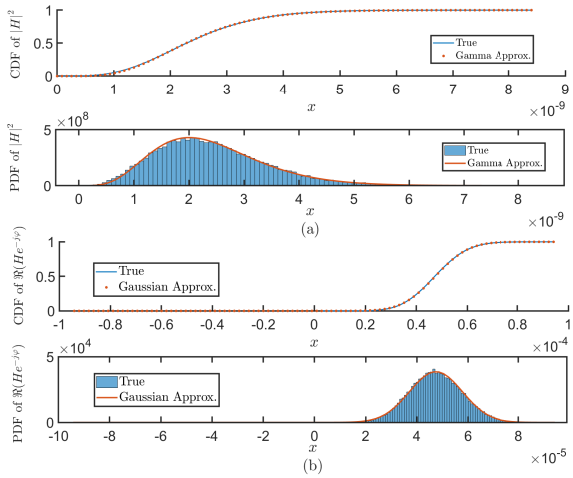

Fig. 4. Fitting the channels distributions by utilizing moment-matching approach. (a) The CDF and PDF of $|H|^2$ in Theorem 1; (b) The CDF and PDF of $\Re\left(He^{-j\varphi}\right)$ in Theorem 2.

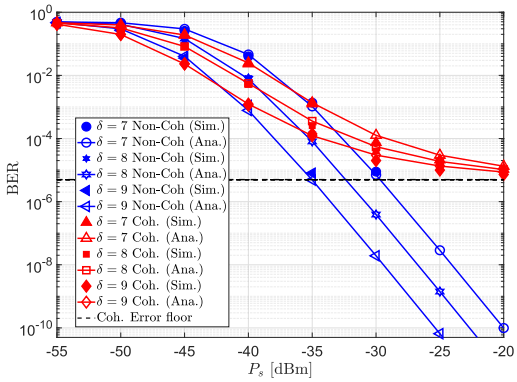

Fig. 5. BER performance versus transmit power P_s of the proposed system with non-coherent and coherent detections, where $Z = 32$, $\varrho = 0.85$, $\sigma^2_{\text{err}} = 0.3$, $p = 3$, and $\delta = 7, 8, 9$.

approximate distributions are obtained by using the moment-matching method. We observed that the approximate CDF and PDF are consistent with true CDF and PDF, respectively, thus validating our developed analysis.

Fig. 5 shows the BER results of the proposed system with non-coherent and coherent detections, where $Z = 32$, $\varrho = 0.85$, $\sigma^2_{\text{err}} = 0.3$, $p = 3$, and $\delta = 7, 8, 9$. We find that, for the same value of δ, coherent detection outperforms non-coherent detection at low transmit power. However, when using a high transmit power, coherent detection is not a preferable method, because as it suffers from the error floor. On the one hand, the RISs are composed of digital circuits that lead to the generation of discrete phase shift. On the other hand, the erroneous channels are generated due to the outdated CSI and imperfect channel estimation. Because of the two aforementioned reasons, coherent detector fails to fully compensate the channel phase, which may make $\Re\left(He^{-j\varphi}\right)$ ultimately become a negative number at the target frequency bin. As a result, the minimum value of the target bin will appear, as shown in Fig. 3 (c), thus incurring detection

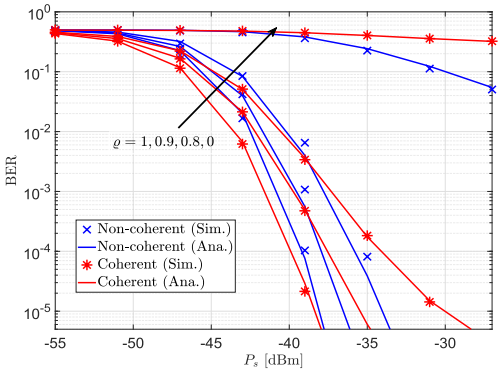

Fig. 6. Impact of the correlation factor ϱ on BER performance of the proposed system with non-coherent and coherent detections, where $Z = 40$, $\sigma^2_{\text{err}} = 0.3$, $p = 3$, and $\delta = 7$.

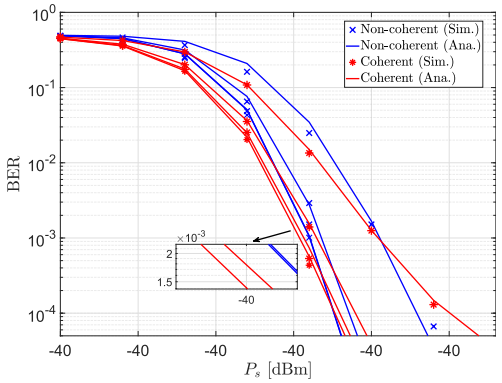

Fig. 7. Impact of the quantization bits p on BER performance of the proposed system with non-coherent and coherent detections, where $Z = 40$, $\varrho = 0.85$, $\sigma^2_{\text{err}} = 0.2$, and $\delta = 7$.

errors. Furthermore, we observe that the BER error floor for coherent detection is independent of spreading factor δ, which is consistent with our analysis.

Fig. 6 illustrates BER performance of the proposed system with non-coherent and coherent detections against the correlation factor ϱ, where $Z = 40$, $\sigma^2_{\text{err}} = 0.3$, $p = 3$, and $\delta = 7$. As shown in Fig. 6, when the CSI is not outdated (i.e., $\varrho = 1$), meaning that the Doppler shift and the channel estimation delay are ignored, BER performance is optimal. However, BER performance deteriorates with a decrease of ϱ decreases, as outdated CSI becomes more severe due to the user mobility and feedback delays, resulting in a lower correlation between the outdated channels and actual channels.

Fig. 7 shows that BER performance of the proposed system with non-coherent and coherent detections against the quantization bits p, where $Z = 40$, $\varrho = 0.85$, $\sigma^2_{\text{err}} = 0.2$, and $\delta = 7$. As shown in Fig. 7, BER performance achieves better as p increases. In addition, we observe that remarkable gains when p increases from 1 to 2 and from 2 to 3. Specifically, for a BER target of 10^{-3}, BER performance can achieve a gain of 5 dBm and 1 dBm when p increases from 1 to 2 and from 2 to 3, respectively. Furthermore, for $p = 3$ (i.e., RISs are made of 3 PIN diodes such that each reflecting element can be represented by eight possible phase shifts), BER performance converges to the continuous phase shifts design of RISs (i.e., p is sufficiently large, set as 100 in Fig. 7).

Fig. 8 shows the effect of the different number of reflecting elements in RISs on BER performance for the proposed system

Authorized licensed use limited to: Universidad Federal de Pernambuco. Downloaded on July 29,2025 at 01:33:53 UTC from IEEE Xplore. Restrictions apply.

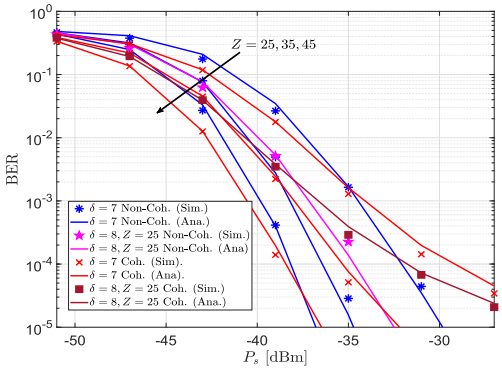

Fig. 8. BER performance of the different number of reflecting elements of RISs for the proposed system with non-coherent and coherent detections, where $\varrho = 0.85$, $\sigma^2_{\text{err}} = 0.2$, $p = 3$, and $\delta = 7$.

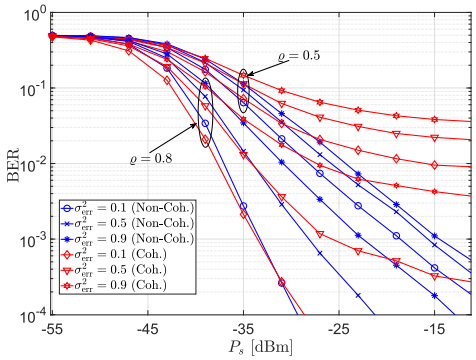

Fig. 9. BER performance of the different variance of the estimation error for the proposed system with non-coherent and coherent detections, where $\varrho = 0.5, 0.8$, $p = 3$, $N = 25$, and $\delta = 7$.

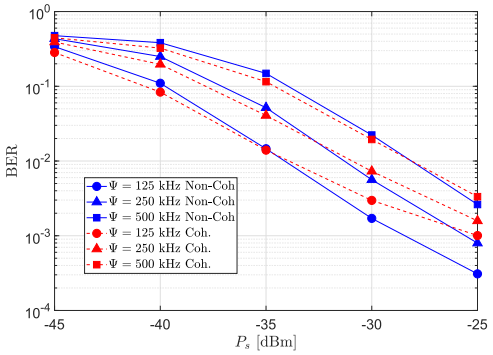

Fig. 10. BER performance of different bandwidths of the proposed system with non-coherent and coherent detections, where $\varrho = 0.8$, $\sigma^2_{\text{err}} = 0.5$, $p = 3$, $N = 25$, and $\delta = 7$.

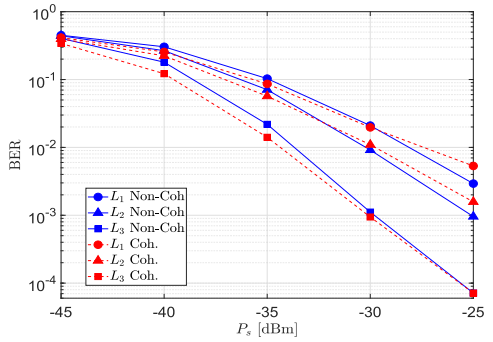

Fig. 11. BER performance of different RIS locations of the proposed system with non-coherent and coherent detections, where $\varrho = 0.95$, $\sigma^2_{\text{err}} = 0.1$, $p = 3$, $N = 80$, and $\delta = 7$.

with non-coherent and coherent detections, where $\varrho = 0.85$, $\sigma^2_{\text{err}} = 0.2$, $p = 3$, and $\delta = 7$. We observe that increasing the value of Z can achieve better BER performance for two detections. Moreover, although a higher SF is frequently used to realize a better BER performance and reach longer transmission range, it results in a long transmission time in the conventional RIS-free system. Therefore, increasing the number of reflective elements allows low SFs to realize the same robustness as high SFs, thereby enhancing the reliability of LoRa systems without reducing the data rate. Specifically, we find that scenario $\delta = 7, Z = 35$ outperforms scenario $\delta = 8, Z = 25$.

Fig. 9 shows the impact of the variance of estimation error on the BER performance for the proposed system with non-coherent and coherent detections, where $\varrho = 0.5, 0.8$, $p = 3$, $N = 25$, and $\delta = 7$. First, as can be seen in Fig. 9, for a fixed ϱ, increasing the variance of estimation error leads to a high BER. This is because a low correlation between the estimated channels and actual channels. In practice, with an increase of the number of transmit pilots, the accuracy of channel estimation improves, while the estimation error declines, which makes it a good way to enhance system performance. In addition, as shown in Fig. 9, increasing the variance of estimation error, deterioration in BER performance is getting more pronounced for a higher value of ϱ. Said differently, for the lower value of ϱ, the impact of channel estimation is less sensitive. It is reasonable to conclude that, when the outdated CSI becomes severe, performing channel estimation on the outdated channels cannot significantly improve performance.

In Fig. 10, we evaluate the BER performance of the proposed system with different bandwidths, where $\varrho = 0.8$, $\sigma^2_{\text{err}} = 0.5$, $p = 3$, $N = 25$, and $\delta = 7$. Bandwidth values for LoRa systems are usually set to 125 kHz, 250 kHz, or 500 kHz according to the IoT applications [3]. Fig. 10 shows that a larger bandwidth degrades the BER performance of the proposed system. This result is reasonable, because a larger bandwidth leads to a higher noise power (refers to the definition of noise variances in paragraph I of this section).

Fig. 11 shows the effect of different RIS locations on BER performance for the proposed system with non-coherent and coherent detections, where $\varrho = 0.95$, $\sigma^2_{\text{err}} = 0.1$, $p = 3$, $N = 80$, and $\delta = 7$. The x coordinates of the four RISs are varied in in the following three considered cases, i.e., Case 1: $L_1 = [2560\ 2570\ 2580\ 2590]$, Case 2: $L_2 = [2760\ 2770\ 2780\ 2790]$, Case 3: $L_3 = [2860\ 2870\ 2880\ 2890]$. Fig. 11 shows that Case 3 yields the best performance while the Case 1 performs the worst. This result is reasonable, because the location of the RIS determines the value of multiplicative path loss. When the RISs move further away from either the gateway or the user, the multiplicative path loss becomes severe. Therefore, in practical scenarios, to overcome this issue, RISs should be deployed close to either the user side or gateway side.

Fig. 12 shows BER comparisons among the conventional RIS-free LoRa system, the RIS-aided LoRa system with blind transmission scheme, and the proposed system, where $\varrho = 0.85$, $\sigma^2_{\text{err}} = 0.1$, $p = 2$, and $\delta = 7$. Of note, the blind transmission scheme does not require CSI, and thus only non-coherent detection is considered. As can be seen in Fig. 12, the proposed system leads a sharp reduction in the BER compared to both

Authorized licensed use limited to: Universidad Federal de Pernambuco. Downloaded on July 29,2025 at 01:33:53 UTC from IEEE Xplore. Restrictions apply.

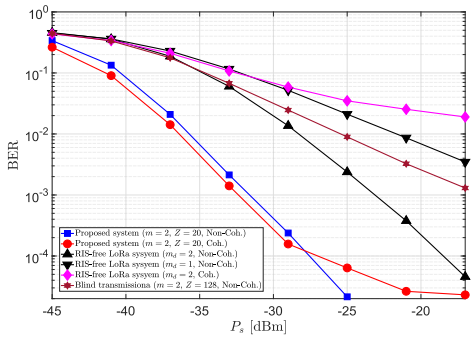

Fig. 12. BER comparisons of the conventional RIS-free LoRa system, the RIS-aided LoRa system adopting blind transmission, and the proposed system, where $\varrho = 0.85$, $\sigma^2_{\text{err}} = 0.1$, $p = 2$, and $\delta = 7$.

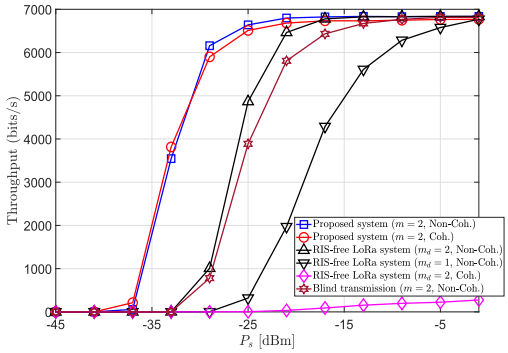

Fig. 13. Throughput comparisons of different LoRa systems, where $\varrho = 0.8$, $\sigma^2_{\text{err}} = 0.85$, $Z = 20$, $p = 2$, and $\delta = 7$.

baseline schemes. Said differently, for a certain BER level, less transmit power is required. In addition, when outdated and imperfect channel estimation are considered in the RIS-free LoRa system, coherent detection not only fails to maintain around 0.7 dB gain as mentioned in [42], but also encounters an error floor at high transmit power. Moreover, as can be seen in Fig. 12, while the RIS-aided LoRa system adopting blind transmission scheme uses a large number of reflecting elements, it has a trivial impact on BER performance. This is because when the blind transmission scheme is adopted, RIS cannot tune the phase shifts, and the signal will be randomly combined at RIS. Furthermore, we observe that the blind transmission scheme outperforms the RIS-free system with the case of $m_d = 1$. However, it is worse than in the case of $m_d = 2$ with a high transmit power. This is because the diversity order of the blind transmission scheme is always one, independent of the number of reflecting elements and fading parameters [11]. Diversity order of the RIS-free system is primarily affected by the fading parameter of the direct link. Therefore, the blind transmission is not a preferable scheme in certain good LoS propagation conditions.

Fig. 13 shows the throughput comparisons among the RIS-aided LoRa system adopting blind transmission, the conventional RIS-free LoRa system, and the proposed system, where $\varrho = 0.8$, $\sigma^2_{\text{err}} = 0.1$, $Z = 20$, $p = 2$, and $\delta = 7$. We find that the throughput of the proposed system reaches its limitation faster than the two baseline schemes. Besides, as mentioned above, with a low transmit power, BER performance of the proposed system with coherent detection is better than the one with non-coherent detection, thus reaching better throughput. However, because of outdated CSI and imperfect channel estimation, coherent detection encounters an

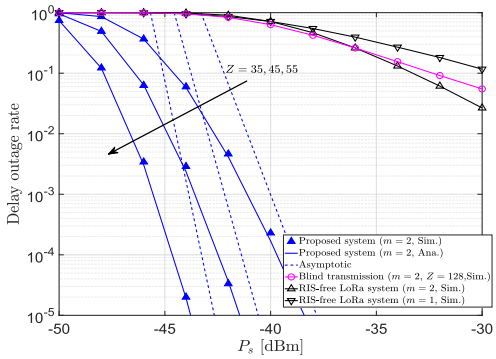

Fig. 14. Impact of different values of Z on the delay outage rate of the proposed system, where $\varrho = 0.9$, $\sigma^2_{\text{err}} = 0.2$, $p = 3$, and $\delta = 7$.

error floor at a high transmit power, thereby causing a lower throughput limitation. In addition, as can be seen in Fig. 13, the RIS-aided LoRa system adopting blind transmission outperforms the conventional RIS-free system with $m_d = 1$ (i.e., Rayleigh fading channel), which is consistent with the results previously reported in [16]. However, in certain good propagation conditions (e.g., $m_d = 2$), the blind transmission scheme does not provide significant gains for throughput. Furthermore, we find that coherent detection is the worst case in terms of throughput in the RIS-free system due to its high error floor.

Fig. 14 shows the effect of different number of reflecting elements on delay outage rate of the proposed system, where $\varrho = 0.9$, $\sigma^2_{\text{err}} = 0.2$, $p = 3$, and $\delta = 7$. The corresponding time threshold is set to 0.0719. We observe that the diversity order matches with the mathematical calculation. In addition, delay outage rate of the proposed system significantly decreases with an increase of the number of reflecting elements. Moreover, we also compare the proposed system with the RIS-aided LoRa system adopting the blind transmission scheme, and the RIS-free LoRa system. The results shows that delay outage rate of the proposed system is better than the one of both baseline schemes, meaning that, within the same transmit power, the proposed system can meet the requirement with lower latency in IoT applications. In addition, the results clearly demonstrate that the proposed system can obtain more diversity gains than the two baseline schemes. Besides, diversity order of two baseline schemes matches the results of our analysis in Section III-C. Namely, the blind transmission scheme is always 1, and the RIS-free LoRa system depends on the fading parameters.

V. Conclusion

In this study, we proposed a generalized multi-RIS-aided LoRa system to resist fading over Nakagami-m fading channels. Since CSI is essential for RIS-aided wireless communication systems, we considered the effect of outdated CSI and imperfect estimated CSI in the proposed system. We also considered discrete phase shift design of RISs. We then used the moment-matching method to obtain the approximate distribution of joint outdated channels and erroneous channels. Moreover, BER, throughput, delay outage rate, and achievable diversity order of the proposed system were derived in closed form. The results revealed that, due to the error floor caused by the erroneous channels, coherent detection is not a preferable

Authorized licensed use limited to: Universidad Federal de Pernambuco. Downloaded on July 29,2025 at 01:33:53 UTC from IEEE Xplore. Restrictions apply.

method for the proposed system in the high SNR regime. Nevertheless, in the presence of the outdated CSI and estimation errors, the proposed system is still superior to RIS-aided LoRa systems adopting blind transmission and conventional RIS-free systems. The reason underlying this outcome is that the proposed system has an excellent diversity gain. In view of these merits, the proposed system can be regarded as an effective solution for future IoT applications. For future work, multiple users will be further considered to meet the requirement of the current LoRa network. Moreover, some optimization problems can be formulated and addressed so that the optimized RIS phase shifts can enhance the reception of the desired signal while suppressing the interference.

APPENDIX A

To facilitate analysis, let $H = U + V + M$, where

$$V = \varrho_d \bar{\nu} \Omega_d \Delta h_d + \sum_{n=1}^{N} \varrho_n \bar{\nu} \mathbf{g}_n \mathbf{\Omega}_n \mathbf{\Phi}_n \Delta \mathbf{h}_n, \tag{45}$$

$$M = \bar{\varrho}_d \Omega_d e_d + \sum_{n=1}^{N} \bar{\varrho}_n \mathbf{g}_n \mathbf{\Omega}_n \mathbf{\Phi}_n \mathbf{e}_n, \tag{46}$$

and $U = U_1 + U_2$ with

$$U_1 = \varrho_d \nu \Omega_d |\tilde{h}_d| e^{-j\phi_d}, \tag{47}$$

$$U_2 = \sum_{n=1}^{N} \sum_{z=1}^{Z_n} \varrho_n \nu \Omega_{n,z} X_{n,z} e^{j(\theta_{n,z} - \phi_d)}. \tag{48}$$

The first moment of $|H|^2$ is given by

$$\mathrm{E}[|H|^2] = \mathrm{E}[|U|^2] + \mathrm{E}[|V|^2] + \mathrm{E}[|M|^2]. \tag{49}$$

Using the property of complex number, $\mathrm{E}\left[|U|^2\right]$ can be computed as

$$\begin{aligned} &\mathrm{E}\left[|U|^2\right] \\ &= \mathrm{E}\left[|U_3 + U_4|^2\right] \\ &= \mathrm{E}[\Re(U_4)^2] + \mathrm{E}\left[U_3^2\right] + 2\mathrm{E}[\Re(U_4)]\mathrm{E}[U_3] + \mathrm{E}[\Im(U_4)^2], \end{aligned} \tag{50}$$

where

$$U_3 = \varrho_d \nu \Omega_d |\tilde{h}_d|, U_4 = \sum_{n=1}^{N} \sum_{z=1}^{Z_n} \varrho_n \nu \Omega_{n,z} X_{n,z} e^{j\theta_{n,z}}. \tag{51}$$

In this study, since we adopts Nakagami-m fading channels, the ℓ-th moment of U_3 is computed as

$$\mathrm{E}\left[U_3^{\ell}\right] = (\varrho_d \nu \Omega_d)^{\ell} \frac{\gamma\left(m_{h_d} + \ell/2\right)}{\gamma\left(m_{h_d}\right) m_{h_d}^{\ell/2}}. \tag{52}$$

Let $U_4 = \sum_{n=1}^{N} \sum_{z=1}^{Z_n} I_{n,z}$ with $I_{n,z} = \varrho_{n,z} \nu \Omega_{n,z} X_{n,z} e^{j\theta_{n,z}}$. $I_{n,z}$ can be decomposed as

$$\begin{aligned} I_{n,z} &= \Re\left(I_{n,z}\right) + j\Im\left(I_{n,z}\right) \\ &= \varrho_{n,z} \nu \Omega_{n,z} X_{n,z} \cos\left(\theta_{n,z}\right) + j\varrho_{n,z} \nu \Omega_{n,z} X_{n,z} \sin\left(\theta_{n,z}\right). \end{aligned} \tag{53}$$

Since $X_{n,z}$ and $\theta_{n,z}$ are mutually independent, and $\theta_{n,z}$ is uniformly distributed in $(-\pi/2^{p_n}, \pi/2^{p_n})$, we obtain

$$\mathrm{E}[\Re(I_{n,z})] = \zeta_n, \mathrm{E}[\Re(I_{n,z})^2] = \left(\frac{1}{2} + \varsigma_n\right) \xi_n, \tag{54}$$

$$\mathrm{E}[\Im(I_{n,z})] = 0, \mathrm{E}[\Im(I_{n,z})^2] = \left(\frac{1}{2} - \varsigma_n\right) \xi_n, \tag{55}$$

where

$$\zeta_n = \sin\left(\frac{\pi}{2^{p_n}}\right) \frac{\varrho_n \nu \Omega_n 2^{p_n} \gamma\left(m_{h_n} + 1/2\right) \gamma\left(m_{g_n} + 1/2\right)}{\pi \gamma\left(m_{h_n}\right) \gamma\left(m_{g_n}\right) m_{h_n}^{1/2} m_{g_n}^{1/2}}, \tag{56}$$

$$\varsigma_n = \frac{2^{p_n - 2}}{\pi} \sin\left(\frac{\pi}{2^{p_n - 1}}\right), \xi_n = \frac{\varrho_n^2 \nu^2 \Omega_n^2 \gamma\left(m_{h_n} + 1\right) \gamma\left(m_{g_n} + 1\right)}{\gamma\left(m_{h_n}\right) \gamma\left(m_{g_n}\right) m_{h_n} m_{g_n}}. \tag{57}$$

For a larger value of Z_n $(n = 1, 2, \ldots, N)$, using the CLT and additivity of the Gaussian distribution, we obtain the approximate distributions of $\Re\left(U_4\right)$ and $\Im\left(U_4\right)$, expressed as

$$\Re\left(U_4\right) \sim \mathcal{N}\left(\lambda_1, \sigma_1^2\right), \Im\left(U_4\right) \sim \mathcal{N}\left(0, \sigma_2^2\right), \tag{58}$$

where

$$\lambda_1 = \sum_{n=1}^{N} Z_n \mathrm{E}[\Re(I_{n,z})] = \sum_{n=1}^{N} Z_n \times \zeta_n, \tag{59}$$

$$\begin{aligned} \sigma_1^2 &= \sum_{n=1}^{N} Z_n \left(\mathrm{E}[\Re(I_{n,z})^2] - \left(\mathrm{E}[\Re\left(I_{n,z}\right)]\right)^2\right) \\ &= \sum_{n=1}^{N} Z_n \times \left[\left(\varsigma_n + \frac{1}{2}\right)\xi_n - \zeta_n^2\right], \end{aligned} \tag{60}$$

$$\sigma_2^2 = \sum_{n=1}^{N} Z_n \mathrm{E}[\Im(I_{n,z})^2] = \sum_{n=1}^{N} Z_n \times \left(\frac{1}{2} - \varsigma_n\right) \xi_n. \tag{61}$$

For $X \sim \mathcal{N}\left(0, \sigma^2\right)$, and $Y = c + X \sim \mathcal{N}\left(c, \sigma^2\right)$ with c being a constant, we have $\mathrm{E}\left[X^{\ell}\right] = \frac{\sigma^{\ell}\Gamma(\ell+1)}{2^{\ell/2}\Gamma(\ell/2+1)}$ if ℓ is even and 0 if odd, and $\mathrm{E}[Y^{\ell}] = \sum_{t=0}^{\ell} \frac{\ell!}{(\ell-t)!t!} c^t \mathrm{E}[X^{\ell-t}]$. Then, we can obtain

$$\mathrm{E}\left[\Re(U_4)^{\ell}\right] = \begin{cases} \sum_{t=0}^{\ell} \frac{\ell!}{(\ell-t)!t!} \times \frac{\sigma_1^{\ell-t}\gamma\left(\ell-t+1\right)}{2^{(\ell-t)/2}\gamma\left(\frac{\ell-t}{2}+1\right)}, & \ell \text{ is even} \\ \sum_{t=0}^{\ell} \frac{\ell!}{(\ell-t)!t!} \times \frac{\sigma_1^{\ell-t}\gamma\left(\ell-t+1\right)}{2^{(\ell-t)/2}\gamma\left(\frac{\ell-t}{2}+1\right)} \\ \quad - \sum_{t=0}^{(\ell-1)/2} \frac{\ell!}{(\ell-2t)!2t!} \lambda_1^{2t} \sigma_1^{\ell-2t}, & \ell \text{ is odd}, \end{cases} \tag{62}$$

$$\mathrm{E}\left[\Im(U_4)^{\ell}\right] = \frac{\sigma_2^{\ell}\Gamma(\ell+1)}{2^{\ell/2}\Gamma(\ell/2+1)}. \tag{63}$$

Therefore, using Eqs. (52), (62) and (63), Eq. (50) can be obtained.

For the RV V, according to the CLT, V can be approximated to a complex Gaussian distribution, i.e., $V \sim \mathcal{CN}\left(0, \sigma_3^2\right)$, where

$$\sigma_3^2 = \varrho_d^2 \bar{\nu}^2 \Omega_d^2 \sigma_{\text{err}}^2 + \sum_{n=1}^{N} Z_n \varrho_n^2 \bar{\nu}^2 \Omega_n^2 \sigma_{\text{err}}^2. \tag{64}$$

Of note, for the RV M, the values of $\mathbf{e}_n$ and e_d variance depend on the corresponding fading parameters of $|\hat{\mathbf{h}}_n|$ and $|\hat{h}_d|$ [23]. Hence, we obtain $\sigma_{n,z}^2 = \sigma_n^2 (z = 1, 2, \ldots, Z_n)$.

Authorized licensed use limited to: Universidad Federal de Pernambuco. Downloaded on July 29,2025 at 01:33:53 UTC from IEEE Xplore. Restrictions apply.

Similarly, we can approximate M as a complex Gaussian distribution by using the CLT, i.e., $M \sim \mathcal{CN}\left(0, \sigma_4^2\right)$, where

$$\sigma_4^2 = \bar{\varrho}_d^2 \Omega_d^2 \sigma_{h_d}^2 + \sum_{n=1}^{N} Z_n \bar{\varrho}_n^2 \Omega_n^2 \sigma_n^2. \tag{65}$$

Therefore, we obtain

$$\mathrm{E}[|V|^2] = \sigma_3^2, \mathrm{E}[|M|^2] = \sigma_4^2. \tag{66}$$

Using Eqs.(50) and (66), $\mathrm{E}[|H|^2]$ in Eq. (49) can be obtained.

The second moment of $|H|^2$ can be obtained as

$$\mathrm{E}\left[|H|^4\right] = \mathrm{E}\left[|U|^4\right] + \mathrm{E}\left[|V+M|^4\right] + 4\mathrm{E}\left[|U|^2\right] \mathrm{E}\left[|V+M|^2\right], \tag{67}$$

where $\mathrm{E}\left[|U|^4\right]$ can be computed as

$$\begin{aligned} \mathrm{E}\left[|U|^4\right] &= \mathrm{E}\left[\Re(U_4)^4\right] + \mathrm{E}\left[U_3^4\right] + 6\mathrm{E}\left[\Re(U_4)^2\right] \mathrm{E}\left[U_3^4\right] \\ &+ 4\mathrm{E}\left[\Re(U_4)\right] \mathrm{E}\left[U_3^3\right] + 4\mathrm{E}\left[\Re(U_4)^3\right] \mathrm{E}\left[U_3\right] \\ &+ 2\mathrm{E}\left[\Im(U_4)^2\right] \mathrm{E}\left[U_3^3\right] + 2\mathrm{E}\left[\Im(U_4)^2\right] \mathrm{E}\left[\Re(U_4)^2\right] \\ &+ 4\mathrm{E}\left[\Re(U_4)\right] \mathrm{E}\left[\Im(U_4)^2\right] \mathrm{E}\left[U_3^3\right] + \mathrm{E}\left[\Im(U_4)^4\right]. \end{aligned} \tag{68}$$

The decomposed terms of $\mathrm{E}\left[|U|^4\right]$ can be obtained by using Eqs. (52), (62), and (63). In addition, from Eq. (67), the sum of two independent Gaussian variables still obeys Gaussian distribution, i.e., $V+M \sim \mathcal{CN}\left(0, \sigma_3^2+\sigma_4^2\right)$. Hence, $|V+M|$ is a Rayleigh random variable, and the ℓ-th moment of $|V+M|$ can be computed as

$$\mathrm{E}\left[|V+M|^{\ell}\right] = \left(\sigma_3^2+\sigma_4^2\right)^{\frac{\ell}{2}} \times \gamma\left(\frac{\ell}{2}+1\right). \tag{69}$$

Hence, combining Eqs. (50), (68), and (69), $\mathrm{E}\left[|H|^4\right]$ in Eq. (67) can be obtained.

The derivation of the first and second moments of $|H|^2$ are completed. Then, using the moment-matching method, we approximate $|H|^2$ as a Gamma distribution with two estimators given in Eq. (26). Finally, the PDF of $|H|^2$ can be expressed as Eq. (25). We finish the proof of Theorem 1.

APPENDIX B

We first focus on the derivation of the first and second moments of $\Re(He^{-j\varphi})$. The first moment of $\Re(He^{-j\varphi})$ can be obtain as

$$\mathrm{E}\left[\Re(He^{-j\varphi})\right] = \mathrm{E}\left[\Re(H_1)\right] + \mathrm{E}\left[\Re(H_2)\right] + \mathrm{E}\left[\Re(H_3)\right], \tag{70}$$

where H_1, H_2 and H_3 are given in Eqs. (16), (17) and (18), respectively. Based on the Appendix A, we have $\Re(H_1) = U_3 + \Re(U_4)$. Hence, the first moment of $\Re(H_1)$ can be computed as

$$\mathrm{E}\left[\Re(H_1)\right] = \varrho_d \nu \Omega_d \frac{\gamma\left(m_{h_d}+1/2\right)}{\gamma\left(m_{h_d}\right) m_{h_d}^{1/2}} + \lambda_1. \tag{71}$$

Since both V and M can be approximated as the Gaussian distribution in Appendix A, $H_2 = Ve^{-j\varphi}$ and $H_3 = Me^{-j\varphi}$ have the same distribution as V and M, respectively, i.e., $H_2 \sim \mathcal{CN}\left(0, \sigma_3^2\right)$, and $H_3 \sim \mathcal{CN}\left(0, \sigma_4^2\right)$. This is because the property of circular symmetry of complex Gaussian, i.e., a complex Gaussian random variable rotated any angle is still a complex Gaussian random variable. As a result, $\Re(H_2) \sim \mathcal{N}\left(0, \frac{1}{2}\sigma_3^2\right)$, $\Re(H_3) \sim \mathcal{N}\left(0, \frac{1}{2}\sigma_4^2\right)$. Hence, we obtain

$$\mathrm{E}\left[\Re(H_2)\right] = 0, \mathrm{E}\left[\Re(H_3)\right] = 0. \tag{72}$$

Therefore, Eq. (70) can be obtained by using Eqs. (71) and (72).

The second moment of $\Re(He^{-j\varphi})$ can be calculated as

$$\mathrm{E}\left[\Re(He^{-j\varphi})^2\right] = \mathrm{E}\left[\Re(H_1)^2\right] + \mathrm{E}\left[\Re(H_2)^2\right] + \mathrm{E}\left[\Re(H_3)^2\right], \tag{73}$$

where

$$\begin{aligned} \mathrm{E}\left[\Re(H_1)^2\right] &= \mathrm{E}\left[U_3^2\right] + \mathrm{E}\left[\Re(U_4)^2\right] + 2\mathrm{E}\left[U_3\right] \mathrm{E}\left[\Re(U_4)\right] \\ &= \varrho_d^2 \nu^2 \Omega_d^2 \frac{\gamma\left(m_{h_d}+1\right)}{\gamma\left(m_{h_d}\right) m_{h_d}} \\ &+ 2\lambda_1 \nu \varrho_d \Omega_d \frac{\gamma\left(m_{h_d}+1/2\right)}{\gamma\left(m_{h_d}\right) m_{h_d}^{1/2}} + \lambda_1 + \sigma_1^2. \end{aligned} \tag{74}$$

Since $\Re(H_2) \sim \mathcal{N}\left(0, \sigma_3^2\right)$ and $\Re(H_3) \sim \mathcal{N}\left(0, \sigma_4^2\right)$, we obtain

$$\mathrm{E}\left[\Re(H_2)^2\right] = \sigma_3^2, \mathrm{E}\left[\Re(H_3)^2\right] = \sigma_4^2. \tag{75}$$

Therefore, Eq. (73) can be obtained by using Eqs. (74) and (75).

We use the moment-matching to approximate $\Re(He^{-j\varphi})$ as the Gaussian distribution with mean λ_3 and variance σ_6^2, i.e., $\Re(He^{-j\varphi}) \sim \mathcal{N}\left(\lambda_3, \sigma_6^2\right)$, where

$$\lambda_3 = \mathrm{E}\left[\Re(H_1)\right] = \varrho_d \nu \Omega_d \frac{\gamma\left(m_{h_d}+1/2\right)}{\gamma\left(m_{h_d}\right) m_{h_d}^{1/2}} + \lambda_1, \tag{76}$$

and

$$\begin{aligned} \sigma_6^2 &= \mathrm{E}\left[\Re(He^{-j\varphi})^2\right] - \left(\mathrm{E}\left[\Re(He^{-j\varphi})\right]\right)^2 = \lambda_1 + \sigma_1^2 + \sigma_3^2 + \sigma_4^2 \\ &+ \frac{\varrho_d^2 \Omega_d^2 \nu^2}{m_{h_d}\left(\gamma(m_{h_d})\right)^2} \left[\gamma(m_{h_d})\gamma(m_{h_d}+1) - \left(\gamma(m_{h_d}+1/2)\right)^2\right]. \end{aligned} \tag{77}$$

We finish the proof of Theorem 2.

REFERENCES

[1] D. C. Nguyen et al., "6G Internet of Things: A comprehensive survey," *IEEE Internet Things J.*, vol. 9, no. 1, pp. 359–383, Jan. 2022.

[2] W. Zhuang, Q. Ye, F. Lyu, N. Cheng, and J. Ren, "SDN/NFV-empowered future IoV with enhanced communication, computing, and caching," *Proc. IEEE*, vol. 108, no. 2, pp. 274–291, Feb. 2020.

[3] O. Afisiadis et al., "On the advantage of coherent LoRa detection in the presence of interference," *IEEE Internet Things J.*, vol. 8, no. 14, pp. 11581–11593, Jul. 2021.

[4] T. Elshabrawy and J. Robert, "Closed-form approximation of LoRa modulation BER performance," *IEEE Commun. Lett.*, vol. 22, no. 9, pp. 1778–1781, Sep. 2018.

[5] H. Ma, G. Cai, Y. Fang, P. Chen, and G. Han, "Design and performance analysis of a new STBC-MIMO LoRa system," *IEEE Trans. Commun.*, vol. 69, no. 9, pp. 5744–5757, Sep. 2021.

Authorized licensed use limited to: Universidad Federal de Pernambuco. Downloaded on July 29,2025 at 01:33:53 UTC from IEEE Xplore. Restrictions apply.

[6] J. Lyu, D. Yu, and L. Fu, "Analysis and optimization for large-scale LoRa networks: Throughput fairness and scalability," *IEEE Internet Things J.*, vol. 9, no. 12, pp. 9574–9590, Jun. 2022.

[7] W. Xu, G. Cai, Y. Fang, S. Mumtaz, and G. Chen, "Performance analysis and resource allocation for a relaying LoRa system considering random nodal distances," *IEEE Trans. Commun.*, vol. 70, no. 3, pp. 1638–1652, Mar. 2022.

[8] M. Di Renzo et al., "Smart radio environments empowered by reconfigurable intelligent surfaces: How it works, state of research, and the road ahead," *IEEE J. Sel. Areas Commun.*, vol. 38, no. 11, pp. 2450–2525, Nov. 2020.

[9] W. Mei and R. Zhang, "Cooperative beam routing for multi-IRS aided communication," *IEEE Wireless Commun. Lett.*, vol. 10, no. 2, pp. 426–430, Feb. 2021.

[10] Q. Li, M. Wen, J. Li, Z. He, and Y. Yan, "Interplay between reconfigurable intelligent surfaces and spatial modulation: New application paradigms," *IEEE Wireless Commun.*, vol. 30, no. 1, pp. 126–133, Feb. 2023.

[11] D. Selimis, K. P. Peppas, G. C. Alexandropoulos, and F. I. Lazarakis, "On the performance analysis of RIS-empowered communications over Nakagami-M fading," *IEEE Commun. Lett.*, vol. 25, no. 7, pp. 2191–2195, Jul. 2021.

[12] K. Xie, G. Cai, G. Kaddoum, and J. He, "Performance analysis and resource allocation of STAR-RIS aided wireless-powered NOMA system," *IEEE Trans. Commun.*, vol. 71, no. 10, pp. 5740–5755, Oct. 2023.

[13] L. Yang, Y. Yang, M. O. Hasna, and M. Alouini, "Coverage, probability of SNR gain, and DOR analysis of RIS-aided communication systems," *IEEE Wireless Commun. Lett.*, vol. 9, no. 8, pp. 1268–1272, Aug. 2020.

[14] G. Xiao, T. Yang, C. Huang, X. Wu, H. Feng, and B. Hu, "Average rate approximation and maximization for RIS-assisted multi-user MISO system," *IEEE Wireless Commun. Lett.*, vol. 11, no. 1, pp. 173–177, Jan. 2022.

[15] S. Lin, B. Zheng, G. C. Alexandropoulos, M. Wen, M. D. Renzo, and F. Chen, "Reconfigurable intelligent surfaces with reflection pattern modulation: Beamforming design and performance analysis," *IEEE Trans. Wireless Commun.*, vol. 20, no. 2, pp. 741–754, Feb. 2021.

[16] X. Zhang et al., "A new reconfigurable intelligent-surface-assisted LoRA system," *IEEE Trans. Veh. Technol.*, vol. 71, no. 8, pp. 9055–9060, Aug. 2022.

[17] Z. Liang, G. Cai, J. He, G. Kaddoum, C. Huang, and M. Debbah, "RIS-enabled anti-interference in LoRA systems," *IEEE Trans. Commun.*, vol. 72, no. 10, pp. 6599–6616, Oct. 2024, doi: 10.1109/TCOMM.2024.3402146.

[18] L. Yang, Y. Yang, D. B. D. Costa, and I. Trigui, "Outage probability and capacity scaling law of multiple RIS-aided networks," *IEEE Wireless Commun. Lett.*, vol. 10, no. 2, pp. 256–260, Feb. 2021.

[19] T. N. Do, G. Kaddoum, T. L. Nguyen, D. B. da Costa, and Z. J. Haas, "Multi-RIS-aided wireless systems: Statistical characterization and performance analysis," *IEEE Trans. Commun.*, vol. 69, no. 12, pp. 8641–8658, Dec. 2021.

[20] D. L. Galappaththige, D. Kudathanthirige, and G. Amarasuriya, "Performance analysis of distributed intelligent reflective surface aided communications," in *Proc. IEEE Global Commun. Conf. (GLOBECOM)*, Dec. 2020, pp. 1–6.

[21] I. Yildirim, E. Basar, and I. F. Akyildiz, "Modeling and analysis of reconfigurable intelligent surfaces for indoor and outdoor applications in future wireless networks," *IEEE Trans. Commun.*, vol. 69, no. 2, pp. 1290–1301, Feb. 2021.

[22] T.-H. Vu and S. Kim, "Performance analysis of full-duplex two-way RIS-based systems with imperfect CSI and discrete phase-shift design," *IEEE Commun. Lett.*, vol. 27, no. 2, pp. 512–516, Feb. 2023.

[23] Y. Zhang, J. Zhang, M. Di Renzo, H. Xiao, and B. Ai, "Reconfigurable intelligent surfaces with outdated channel state information: Centralized vs. distributed deployments," *IEEE Trans. Commun.*, vol. 70, no. 4, pp. 2742–2756, Apr. 2022.

[24] Z. Xie, W. Yi, X. Wu, Y. Liu, and A. Nallanathan, "Downlink multi-RIS aided transmission in backhaul limited networks," *IEEE Wireless Commun. Lett.*, vol. 11, no. 7, pp. 1458–1462, Jul. 2022.

[25] P. Yang, L. Yang, and S. Wang, "Performance analysis for RIS-aided wireless systems with imperfect CSI," *IEEE Wireless Commun. Lett.*, vol. 11, no. 3, pp. 588–592, Mar. 2022.

[26] X. Zhu et al., "Reconfigurable-intelligent-surface-aided space-shift keying with imperfect CSI," *IEEE Internet Things J.*, vol. 11, no. 7, pp. 11480–11495, Apr. 2024.

[27] C. Liu, X. Liu, D. W. K. Ng, and J. Yuan, "Deep residual learning for channel estimation in intelligent reflecting surface-assisted multi-user communications," *IEEE Trans. Wireless Commun.*, vol. 21, no. 2, pp. 898–912, Feb. 2022.

[28] A. Bansal, N. Agrawal, K. Singh, C.-P. Li, and S. Mumtaz, "RIS selection scheme for UAV-based multi-RIS-aided multiuser downlink network with imperfect and outdated CSI," *IEEE Trans. Commun.*, vol. 71, no. 8, pp. 4650–4664, Aug. 2023.

[29] T. K. Nguyen, H. H. Nguyen, and E. Bedeer, "Performance improvement of LoRa modulation with signal combining and semi-coherent detection," *IEEE Commun. Lett.*, vol. 25, no. 9, pp. 2889–2893, Sep. 2021.

[30] J.-M. Kang and K. W. Choi, "Efficient demodulation algorithms for MIMO-LoRa," *IEEE Internet Things J.*, vol. 10, no. 23, pp. 21129–21130, Dec. 2023.

[31] Q. Li, M. Wen, and M. D. Renzon, "Single-RF MIMO: From spatial modulation to metasurface-based modulation," *IEEE Wireless Commun.*, vol. 28, no. 4, pp. 88–95, Aug. 2021.

[32] C. Huang, R. Mo, and C. Yuen, "Reconfigurable intelligent surface assisted multiuser MISO systems exploiting deep reinforcement learning," *IEEE J. Sel. Areas Commun.*, vol. 38, no. 8, pp. 1839–1850, Aug. 2020.

[33] C. Huang, A. Zappone, G. C. Alexandropoulos, M. Debbah, and C. Yuen, "Reconfigurable intelligent surfaces for energy efficiency in wireless communication," *IEEE Trans. Wireless Commun.*, vol. 18, no. 8, pp. 4157–4170, Aug. 2019.

[34] L. Wei, C. Huang, G. C. Alexandropoulos, C. Yuen, Z. Zhang, and M. Debbah, "Channel estimation for RIS-empowered multi-user MISO wireless communications," *IEEE Trans. Commun.*, vol. 69, no. 6, pp. 4144–4157, Jun. 2021.

[35] E. Basar, U. Aygolu, E. Panayirci, and H. V. Poor, "Performance of spatial modulation in the presence of channel estimation errors," *IEEE Commun. Lett.*, vol. 16, no. 2, pp. 176–179, Feb. 2012.

[36] J. Wu and C. Xiao, "Optimal diversity combining based on linear estimation of Rician fading channels," *IEEE Trans. Commun.*, vol. 56, no. 10, pp. 1612–1615, Oct. 2008.

[37] G. Pasolini, "On the LoRa chirp spread spectrum modulation: Signal properties and their impact on transmitter and receiver architectures," *IEEE Trans. Wireless Commun.*, vol. 21, no. 1, pp. 357–369, Jan. 2022.

[38] LoRa Alliance. (2020). *LoRaWAN 1.0.4 Specification*. [Online]. Available: https://resources.lora-alliance.org/technical-specifications/ts001-1-0-4-lor%awan-l2-1-0-4-specification

[39] M. Xhonneux, O. Afisiadis, D. Bol, and J. Louveaux, "A low-complexity LoRa synchronization algorithm robust to sampling time offsets," *IEEE Internet Things J.*, vol. 9, no. 5, pp. 3756–3769, Mar. 2022.

[40] S. Atapattu et al., "Reconfigurable intelligent surface assisted two-way communications: Performance analysis and optimization," *IEEE Trans. Commun.*, vol. 68, no. 10, pp. 6552–6567, Oct. 2020.

[41] J. Li et al., "Index modulation multiple access for 6G communications: Principles, applications, and challenges," *IEEE Netw.*, vol. 37, no. 1, pp. 52–60, Jan. 2023.

[42] T. Elshabrawy, P. Edward, M. Ashour, and J. Robert, "On the different mathematical realizations for the digital synthesis of LoRa-based modulation," in *Proc. 25th Eur. Wireless Conf.*, May 2019, pp. 1–6.

[43] S. Al-Ahmadi and H. Yanikomeroglu, "On the approximation of the generalized-K distribution by a gamma distribution for modeling composite fading channels," *IEEE Trans. Wireless Commun.*, vol. 9, no. 2, pp. 706–713, Aug. 2010.

[44] D. Zwillinger and A. Jeffrey, *Table of Integrals, Series, and Products*. Amsterdam, The Netherlands: Elsevier, 2007.

[45] F. Turinovi, J. Vukovi, S. Boo, and G. Iul, "Analysis of LoRa parameters in real-world communication," in *Proc. Pro. Int. Symp. (ELMAR)*, Sep. 2020, pp. 87–90.

[46] Z. Wang, B. Lin, Q. Ye, Y. Fang, and X. Han, "Joint computation offloading and resource allocation for maritime MEC with energy harvesting," *IEEE Internet Things J.*, vol. 11, no. 11, pp. 19898–19913, Jun. 2024.

[47] P. T. Tran, B. C. Nguyen, T. M. Hoang, and T. N. Nguyen, "On performance of low-power wide-area networks with the combining of reconfigurable intelligent surfaces and relay," *IEEE Trans. Mob. Comput.*, vol. 22, no. 10, pp. 6086–6096, Oct. 2023.

[48] G. M. Bianco, R. Giuliano, G. Marrocco, F. Mazzenga, and A. Mejia-Aguilar, "LoRa system for search and rescue: Path-loss models and procedures in mountain scenarios," *IEEE Internet Things J.*, vol. 8, no. 3, pp. 1985–1999, Feb. 2021.

Authorized licensed use limited to: Universidad Federal de Pernambuco. Downloaded on July 29,2025 at 01:33:53 UTC from IEEE Xplore. Restrictions apply.

Zhaokun Liang received the B.Sc. degree in communication engineering from Northeast Electric Power University, Jilin, China, in 2020. He is currently pursuing the M.Sc. degree in information and communication engineering with Guangdong University of Technology, Guangzhou, China. His primary research interests include spread-spectrum modulation, reconfigurable intelligent surface, and the Internet of Things.

Guofa Cai (Senior Member, IEEE) received the B.S. degree in communication engineering from Jimei University, Xiamen, China, in 2007, the M.S. degree in circuits and systems from Fuzhou University, Fuzhou, China, in 2012, and the Ph.D. degree in communication engineering from Xiamen University, Xiamen, in 2015. In 2017, he was a Research Fellow with the School of Electrical and Electronic Engineering, Nanyang Technological University, Singapore. He is currently a Full Professor with the School of Information Engineering, Guangdong University of Technology, China. His primary research interests include information theory and coding, spread-spectrum modulation, wireless body area networks, and the Internet of Things.

Jiguang He (Senior Member, IEEE) received the Ph.D. degree in communications engineering from the University of Oulu, Finland, in 2018. He is currently an Associate Professor with Great Bay University, Dongguan, Great Bay Area, China, and holds a Docentship (a.k.s Adjunct Professor) with the University of Oulu. From September 2013 to March 2015, he was affiliated with the State Key Laboratory of Terahertz and Millimeter Waves, City University of Hong Kong. From June 2015 to August 2021, he was associated with the Centre for Wireless Communications (CWC), University of Oulu, initially as a Doctoral Researcher and later as a Post-Doctoral Researcher. He was an Assistant Professor with Macau University of Science and Technology from August 2021 to March 2022, and a Senior Researcher with the Technology Innovation Institute from March 2022 to August 2024. He has actively contributed to several international and national projects, including EU FP7 RESCUE, EU H2020 ARIADNE, and the 6G Flagship. He received one FDCT-GDST Joint Research Project from Macau Science and Technology Development Fund. His research interests span integrated sensing and communications, reconfigurable intelligent surfaces, mmWave/THz communications, and AI for communications and networking. He received the Best Paper Award from IEEE ICCT 2023 and IEEE ICC Workshop 2024. He is recognized as an Exemplary Reviewer for IEEE TRANSACTIONS ON COMMUNICATIONS and IEEE COMMUNICATIONS LETTERS. He serves as a technical program committee (TPC) member for various IEEE conferences. Currently, he serves as an Associate Editor for IEEE TRANSACTIONS ON VEHICULAR TECHNOLOGY.

Georges Kaddoum (Senior Member, IEEE) received the bachelor's degree in electrical engineering from the École Nationale Supérieure de Techniques Avancées (ENSTA Bretagne), Brest, France, the M.S. degree in telecommunications and signal processing (circuits, systems, and signal processing) from the Université de Bretagne Occidentale and Telecom Bretagne (ENSTB), Brest, in 2005, and the Ph.D. degree (Hons.) in signal processing and telecommunications from the National Institute of Applied Sciences (INSA), University of Toulouse, Toulouse, France, in 2009. He is currently a Professor and the Research Director of the Resilient Machine Learning Institute (ReMI) and an Industrial Research Chair and the Tier 2 Canada Research Chair of the École de Technologie Supérieure (ÉTS), Université du Québec, Montréal, Canada. He has published over more than 300 journals, conference papers, two chapters in books, and has eight pending patents. His current research interests include wireless communication networks, tactical communications, resource allocations, and network security. He received the Best Papers Awards at the 2014 IEEE International Conference on Wireless and Mobile Computing, Networking, Communications (WIMOB); the 2017 IEEE International Symposium on Personal Indoor and Mobile Radio Communications (PIMRC); and the 2023 IEEE International Wireless Communications and Mobile Computing Conference (IWCMC). Moreover, he received the IEEE Transactions on Communications Exemplary Reviewer Award in 2015, 2017, and 2019; the Research Excellence Award of the Université du Québec in 2018; and the Research Excellence Award from ÉTS in 201 in recognition of his outstanding research outcomes. He also won the 2022 IEEE Technical Committee on Scalable Computing (TCSC) Award for Excellence (Middle Career Researcher). Lastly, he has received the prestigious 2023 MITACS Award for Exceptional Leadership. He served as an Associate Editor for IEEE TRANSACTIONS ON INFORMATION FORENSICS AND SECURITY and IEEE COMMUNICATIONS LETTERS. He is currently serving as an Area Editor for IEEE TRANSACTIONS ON MACHINE LEARNING IN COMMUNICATIONS AND NETWORKING and an Editor for IEEE TRANSACTIONS ON COMMUNICATIONS.

Chongwen Huang (Member, IEEE) received the B.Sc. degree from Nankai University in 2010, the M.Sc. degree from the University of Electronic Science and Technology of China in 2013, and the Ph.D. degree from Singapore University of Technology and Design (SUTD) in 2019. From October 2019 to September 2020, he was a Post-Doctoral Researcher with SUTD. In September 2020, he joined Zhejiang University, as a tenure-track young Professor. His main research interests are focused on holographic MIMO surface/reconfigurable intelligent surface, B5G/6G wireless communications, mmWave/THz communications, and deep learning technologies for wireless communications. He was a recipient of the 2021 IEEE Marconi Prize Paper Award, the 2023 IEEE Fred W. Ellersick Prize Paper Award, and the 2021 IEEE ComSoc Asia-Pacific Outstanding Young Researcher Award. He has been served as an Editor for IEEE COMMUNICATIONS LETTER, *Signal Processing* (Elsevier), *EURASIP Journal on Wireless Communications and Networking*, and *Physical Communication*, since 2021.

Authorized licensed use limited to: Universidad Federal de Pernambuco. Downloaded on July 29,2025 at 01:33:53 UTC from IEEE Xplore. Restrictions apply.